KUOPION YLIOPISTON JULKAISUJA C. LUONNONTIETEET JA YMPÄRISTÖTIETEET 239
KUOPIO UNIVERSITY PUBLICATIONS C. NATURAL AND ENVIRONMENTAL SCIENCES 239

JATTA BERBERAT NÉE KURKIJÄRVI

Quantitative Magnetic Resonance Imaging of Native and Repaired Articular Cartilage

An Experimental and Clinical Approach

Doctoral dissertation

To be presented by permission of the Faculty of Natural and Environmental Sciences
of the University of Kuopio for public examination in
Auditorium L21, Snellmania building, University of Kuopio
on Tuesday 23rd September 2008, at 12 noon

Department of Physics and
Institute of Biomedicine, Anatomy
University of Kuopio

KUOPION YLIOPISTO

KUOPIO 2008

Distributor: Kuopio University Library
P.O. Box 1627
FI-70211 KUOPIO
FINLAND
Tel. +358 40 355 3430
Fax +358 17 163 410
http://www.uku.fi/kirjasto/julkaisutoiminta/julkmyyn.html

Series Editors: Professor Pertti Pasanen, Ph.D.
Department of Environmental Science

Professor Jari Kaipio, Ph.D.
Department of Physics

Author's address: Department of Physics
University of Kuopio
P.O. Box 1627
FI-70211 KUOPIO
FINLAND
Tel. +41 79 277 62 32
Fax +358 17 162 585
E-mail: jattaberberat@gmail.com

Supervisors: Professor Jukka Jurvelin, Ph.D.
Department of Physics
University of Kuopio

Docent Miika Nieminen, Ph.D.
Department of Diagnostic Radiology
Oulu University Hospital

Reviewers: Docent Antero Koivula, Ph.D.
Department of Oncology and Radiotherapy
Oulu University Hospital

Vládimir Mlynárik, Ph.D.
Laboratory of Functional and Metabolic Imaging
Ecole Polytechnique Fédérale de Lausanne
Lausanne, Switzerland

Opponent: Assistant Professor Young-Jo Kim, M.D., Ph.D.
Harvard Medical School
Boston, MA, USA

ISBN 978-951-27-0977-9
ISBN 978-951-27-1092-8 (PDF)
ISSN 1235-0486

Kopijyvä
Kuopio 2008
Finland

Berberat née Kurkijärvi, Jatta. Quantitative Magnetic Resonance Imaging of Native and Repaired Articular Cartilage: An Experimental and Clinical Approach. Kuopio University Publications C. Natural and Environmental Sciences 239. 2008. 90 p.
ISBN 978-951-27-0977-9
ISBN 978-951-27-1092-8 (PDF)
ISSN 1235-0486

ABSTRACT

Degenerative joint diseases, such as osteoarthritis (OA), and trauma–based knee injuries damage the articular cartilage. Consequently, the joint function becomes impaired and severe pain decreases the quality of life of countless individuals. Quantitative magnetic resonance imaging (qMRI) is the only non-invasive technique available which can evaluate the structural and compositional properties of articular cartilage. In this study, three quantitative ^{1}H NMR relaxation techniques were investigated *in vitro* at 9.4 T using human and bovine cartilage and *in vivo* at 1.5 T in orthopaedic patients.

In the present study, T_1 and T_2 relaxation times and Gd-DTPA^{2-}–enhanced MRI of cartilage (dGEMRIC) techniques were used to assess the ability of these techniques to probe the structural and mechanical properties across the cadaver human knee joint, and the results were compared with histological reference techniques (i.e. polarized light microscopy (PLM) and optical density (OD) microscopy) and mechanical testing. The reproducibility of T_2 measurement *in vitro* was examined in bovine articular cartilage. The structure of cartilage was studied with T_2 in the presence of Gd-DTPA^{2-}. The ability of native T_1 to reflect tissue hydration was evaluated. Finally, the ability of T_2 and dGEMRIC to evaluate *in vivo* regeneration of cartilage tissue after autologous chondrocyte transplantation (ACT) was assessed in patients at 10–15 months after surgery.

MRI techniques reproduced satisfactorily the variations in mechanical properties in human tissue. The mean thicknesses of the different cartilage zones were consistent when determined from T_2 and PLM profiles. The characteristic laminar cartilage structure, as detected consistently with PLM and T_2, was preserved in the presence of Gd-DTPA^{2-}. The reproducibility of T_2 measurements was good. T_1 relaxation rate displayed a high linear association with the cartilage water content. ACT grafts showed a general trend towards longer T_2 values for bulk tissue as well as for the superficial and deep tissue as compared to the adjacent native cartilage. dGEMRIC detected no significant differences between the native cartilage and graft tissue.

The present results demonstrate that qMRI can serve as a biomarker for structural (collagen network architecture), compositional (*i.e.* proteoglycan and water content) and mechanical (compressive stiffness) properties of articular cartilage. Further, by combining different quantitative magnetic resonance imaging techniques it is possible to achieve a comprehensive characterization of native cartilage and cartilage repair.

National Library of Medicine Classification: WE 103, WE 300, WE 304, WE 348, WN 185
Medical Subject Headings: Joint Diseases/diagnosis; Osteoarthritis/diagnosis; Cartilage, Articular; Magnetic Resonance Imaging; Contrast Media; Gadolinium DTPA; Biomechanics; Histology; Microscopy, Polarization; Transplantation, Autologous; Chondrocytes; Collagen; Proteoglycans

To my dearest Tarcis, Janina and Olivia

ACKNOWLEDGEMENTS

This work was carried out in the Department of Physics, University of Kuopio, the Institute of Biomedicine, the Department of Anatomy, University of Kuopio and the Department of Biomedical NMR, A. I. Virtanen Institute, University of Kuopio. I wish to express my deepest gratitude to everyone who has contributed to this thesis and helped me throughout the study. Especially, I wish to mention the following persons.

First, I would like to issue my warm thanks to my first supervisor Professor Jukka Jurvelin, Ph.D. With his enthusiasm, support and professional supervision, he has guided me through this thesis. It has been a privilege to work in his group.

I owe my deepest gratitude to my second supervisor, Docent Miika Nieminen, Ph.D. Without his support, encouragement and professional guidance, this work would not exist. It has been very enlightening to work under his supervision.

This study would not have been possible without the help of Mikko Nissi, Ph.D. I wish to thank him for his friendship, comments and technical assistance he has offered to improve this study.

I wish to express my sincere thanks to Professor Heikki Helminen, M.D., Ph.D., for the opportunity to carry out the experiments in the Department of Anatomy. I thank Professor Ilkka Kiviranta, M.D., Ph.D., Anna Vasara, M.D., Ph.D., Risto Ojala M.D., Ph.D. and Lauri Mattila, M.D. for their support and medical expertise they shared with me during this work. I also wish to thank Professor Mikko Lammi, Ph.D. for his help and quidance on biochemistry used in this study.

I thank the official reviewers of this thesis, Vladimir Mlynárik, Ph.D., and Antero Koivula, Ph.D., for their comments and constructive criticism. I am also grateful to Ewen MacDonald, D.Pharm., for the linguistic review.

I owe many thanks to my friends and collaborators, who have helped and participated in this study. I want to thank the people working in the Institute of Biomedicine, Department of Anatomy in Kuopio, especially Mrs. Eija Rahunen and Mr. Kari Kotikumpu. I also want to express my gratitude to our BBC-group researchers Eveliina Lammentausta, Ph.D., Juha Töyräs, Ph.D., Mikko Laasanen, Ph.D., Simo Saarakkala, Ph.D. and Jarno Rieppo, M.D. for their ideas and cheerful support. Panu Kiviranta, M.D. has been wonderful in helping me to find missing references, and for the great spirit of the BBC-group I would like to thank Rami Korhonen, Ph.D., Mikko Hakulinen, Ph.D., Heikki Nieminen, Ph.D., Jani Hirvonen, M.Sc., Petro Julkunen, Ph.D., Hanna Isaksson, Ph.D., Erna Kaleva, M.Sc., Antti Aula, M.Sc., Janne Karjalainen, M.Sc., Ossi Riekkinen, M.Sc., Tuomo Silvast, M.Sc., Matti Timonen, B.Sc. and Pauno Lötjönen, B.Sc. The fellowship in this group has been something really special and the atmosphere has given me strength and joy to complete this work. I also want to thank the co-authors for their contributions to this study. I owe my thanks to Keski-Suomen Magneetti Oy, Jyväskylä, Finland, and their personnel for contributing data for the *in vivo* part of the thesis, as well as Atria Lihakunta Oyj, Kuopio, Finland, for providing bovine joints as research material. I also want to address my gratitude to Department of Biomedical NMR, A. I. Virtanen Institute, for providing the NMR facilities for the studies, especially the following persons: Professor Risto Kauppinen, M.D., Ph.D., Docent Olli Gröhn, Ph.D. and Johanna Närväinen, Ph.D. I would also like to thank Docent Juhana Hakumäki, M.D., Ph.D. for his guidance and support on this project.

I am grateful to my parents, Mikko and Pirjo, for their encouragement and continuous support of this work. I am also grateful to my brothers, Antti and Timo, whose cheerful spirit and encouragement shone into this project. I want to thank my daughters,

Janina and Olivia, who were patient and understanding for these endless hours I spent next to the computer. Finally, I want to thank my beloved husband, Tarcis, for his support and patience throughout this project. He has lived with me the ups and downs of this project. His love made this work possible. Last, I want to thank our *au pair*, Johanna, for taking such kind care of my little girls so I could concentrate on the thesis.

Financial support from Kuopio University Hospital (EVO 5031329); Jyväskylä Central Hospital (EVO BO204); Academy of Finland (grant 205886), National Graduate School of Musculoskeletal Disorders and Biomaterials, Kuopio University Foundation, the Finnish Academy of Science and Letters, Paulo Research Foundation and Finnish Cultural Foundation of Northern Savo is gratefully acknowledged.

Rothrist, Switzerland, September, 2008

Jatta Berberat

ABBREVIATIONS AND NOMENCLATURE

ACT	autologous chondrocyte transplantation
ADC	apparent diffusion constant
BF	optical birefringence of polarized light
CV	coefficient of variation
dGEMRIC	delayed Gadolinium Enhanced MRI of Cartilage
DTI	diffusion tensor imaging
ECM	extracellular matrix
EDTA	ethylenediaminetetraacetic acid
ETL	echo train length
FCD	fixed charge density
FT	Fourier transform
FG	femoral groove
FID	free induction decay
FLC	lateral condyle of femur
FMC	medial condyle of femur
FOV	field of view
FSE	fast spin echo sequence
GAG	glycosaminoglycans
Gd–DTPA^{2-}	gadolinium diethylene triamine pentaacetic acid
$[\text{Gd–DTPA}]_b$	molar concentration of Gd–DTPA in bath
$[\text{Gd–DTPA}]_t$	molar concentration of Gd–DTPA in tissue
LPG	lateral patellar groove
MACT	matrix–associated autologous chondrocyte transplantation
MR	magnetic resonance
MRI	magnetic resonance imaging
MT	magnetization transfer
n	number of samples
NMR	nuclear magnetic resonance
OA	osteoarthritis
OCD	osteochondritis dissecans
OD	optical density microscopy of Safranin–O stained PGs
p	statistical significance
PAT	patella
PBS	phosphate saline buffer
PD	proton density
PG	proteoglycan
PLM	polarized light microscopy
qMRI	quantitative magnetic resonance imaging

RF	radio frequency
ROI	region of interest
SD	standard deviation
SI	signal intensity
TE	echo time
TI	inversion time
TLP	lateral tibial plateau
TMP	medial tibial plateau
TR	repetition time

a_F	optical constant
A	atomic mass number
A_l	absorbance
b_F	optical constant
B	magnetic field strength
B_{ext}	external magnetic field
B_z	magnetic field in z–direction
B_0	static magnetic field strength
B_1	rf–pulse field strength
E	energy between nuclei states
E_{eq}	Young's modulus
f_0	Larmor frequency
G_d	dynamic modulus
G_1	storage modulus
G_2	loss modulus
H_A	aggregate modulus
H_2O	water content
I	intensity
I_0	initial intensity
M_s	quantum number corresponding to angular momentum operator
M_x	magnetization components along x–axis
M_{xy}	magnetization components along xy–plane
M_y	magnetization components along y–axis
M_z	magnetization components along z–axis
M_0	equilibrium magnetization vector
k	Boltzmann's constant
l	optical path length
N	number of nuclei in the spin orientation
r	Pearson correlation coefficient
R	relaxivity

R_1	T_1 relaxation rate
R_2	T_2 relaxation rate
s	spin
t	time
T_1	spin–lattice relaxation time
$T_{1\mathrm{Gd}}$	spin–lattice relaxation time in presence of Gd–DTPA^{2-}
$T_{1\rho}$	spin–lattice relaxation time in rotating frame
$T_{2\mathrm{Gd}}$	spin–spin relaxation time in presence of Gd–DTPA^{2-}
T_l	transmittance
T_2	spin–spin relaxation time
T_2'	component of T_2 relaxation time induced by field inhomogeneities
T_2^*	total spin–spin relaxation time
α	rotation angle of polarized light
γ	gyromagnetic ratio
ϵ	axial strain
ϵ_l	lateral strain
λ	wavelength
μ	magnetic dipole moment
ν	Poisson's ratio
σ	stress
σ_d	dynamic stress
τ_c	correlation time
ω_0	angular Larmor frequency
$\hbar$	Planck's constant
Z	number of protons in a nucleus

LIST OF ORIGINAL PUBLICATIONS

This thesis is based on the following original articles referred by their Roman numerals:

I J. E. Kurkijärvi, M. J. Nissi, I. Kiviranta, J. S. Jurvelin and M. T. Nieminen. Delayed Gadolinium-Enhanced MRI of Cartilage (dGEMRIC) and T_2 Characteristics of Human Knee Articular Cartilage: Topographical Variation and Relationships to Mechanical Properties. *Magn Reson Med* 52:41-46, 2004.

II J. E. Kurkijärvi, M. J. Nissi, J. Rieppo, J. Töyräs, I. Kiviranta, M. T. Nieminen and J. S. Jurvelin. The zonal architecture of human articular cartilage described by T_2 relaxation time in the presence of Gd-DTPA^{2-}. *Magn Reson Imaging* 26:602-607, 2008.

III J. E. Berberat, M. J. Nissi, J. S. Jurvelin and M. T. Nieminen. Assessment of Interstitial Water Content of Articular Cartilage with T_1 Relaxation. *submitted to Magn Reson Imaging*.

IV J. E. Kurkijärvi, L. Mattila, R. O. Ojala, A. Vasara, J. S. Jurvelin, I. Kiviranta and M. T. Nieminen. Evaluation of cartilage repair in the distal femur after autologous chondrocyte transplantation using T_2 relaxation time and dGEMRIC. *Osteoarthritis and Cartilage* 15:372-378, 2007.

CONTENTS

CHAPTER I

Introduction

Osteoarthritis (OA) causes pain and functional disability in countless individuals. OA disrupts the cartilage tissue, increases the water content in the tissue and thickens the subchondral bone [27]. These degenerative changes reduce cartilage stiffness, and impair the mechanical function of the joint [4].

Cartilage lacks the capacity to repair and heal the damage spontaneously. Therefore, early diagnosis of cartilage degradation is important in order to slow down OA progression and to reduce pain and other symptoms of the patients with suitable treatments. In trauma–based acute cartilage injuries, but not in OA patients, one treatment method is surgical cartilage repair.

Conventional methods, such as X–ray imaging of the joint and arthroscopy, are too insensitive to detect the early OA changes and the latter is invasive. Clinically, a non–invasive diagnostic technique is desirable that would permit the differentiation between different stages of cartilage generation with reproducible results. Furthermore, the ideal technique would be quick to perform and be inexpensive.

Macromolecular changes in tissues are reflected in the magnetic properties of water protons, and therefore magnetic resonance imaging (MRI) represents a non-invasive method to detect early changes in articular cartilage. In particular, ^{1}H nuclear magnetic resonance (NMR) relaxation properties provide multifaceted information about cartilage structure, composition and function [13, 64, 107, 134, 135, 189, 198].

In this thesis, high field MRI was used to extend the previous *in vitro* cartilage research, particularly aiming to apply and test quantitative MRI techniques in human articular cartilage and to elucidate variations in the properties of native and repaired human articular cartilage. Furthermore, different MRI techniques were used to assess their ability to probe the

structural and mechanical properties of human cartilage. The possibility to merge different quantitative MRI procedures into one contrast agent imaging session was also evaluated. The water content of articular cartilage was estimated by MRI. Finally, quantitative MRI methods were applied *in vivo* in patients undergoing cartilage repair.

CHAPTER II

Articular cartilage

2.1 Structure and composition

Our knee joints are subjected to very high mechanical loads, up to ten times one's own body weight [129]. As the human knee joint may be exposed to one million cycles of loading per year [129], a complex interplay between structural, compositional and mechanical properties of cartilage tissue is needed to carry out this demanding mechanical task. This represents the main role in reducing the mechanical friction and minimizing stresses occurring during joint motion [28].

Articular cartilage, *i.e.* hyaline cartilage, has a smooth and glistening white appearance. There are no blood vessels or nerves in articular cartilage. Articular cartilage contains a solid matrix (*i.e.* chondrocytes, collagen and proteoglycan (PG)) and fluid (*i.e.* interstitial water and electrolytes) (figure 2.1, table 2.1). Chondrocytes are metabolically active and synthesize, organize and degrade matrix components. The collagen fibers resist tensile stresses, bind PGs and limit tissue swelling. About 90% of the collagen in articular cartilage is of type II, organized in a triple helix structure of three polypeptide chains [170]. These fibers have poor stretching properties, but the bending ability of collagen is excellent. Collagen fibers supplement the support structure of articular cartilage, and PGs and chondrocytes are bonded within the three–dimensional collagen matrix.

Proteoglycan chains form large aggregate molecules by linking themselves with hyaluronic acid through the link protein [130]. This aggrecan molecule contains laterally attached, electronegatively charged chondroitin- and keratan–sulfated glycosaminoglycan (GAG) chains. They attract water and sodium ions, causing an osmotic pressure that keeps the cartilage structure stable [66]. The charged groups, referred to as a fixed charge

density (FCD), create also strong repulsive forces against each other [129].

The amount of interstitial water depends mainly on FCD (affected by PGs), swelling pressure (collagen–PG), the organization of collagen network and the mechanical strength of the collagen–PG solid matrix (table 2.2) [129]. A major fraction of the water is free to move, a small amount is contained in chondrocytes while 60-70% of water exists around proteoglycan aggregates [114, 130].

Articular cartilage is structurally inhomogeneous and can be divided into four different zones (figure 2.1). In the superficial zone, collagen fibers run parallel to the cartilage surface and the chondrocytes are flattened, water concentration is at its highest level and the proteoglycan content at its lowest level. In the intermediate zone, collagen fibers are randomly organized and the chondrocytes are round in shape. The water content and the chondrocyte concentration are lower than in the superficial zone. The proteoglycan content is higher than in the superficial zone. In the deep zone, collagen fibers run perpendicular to the articular surface and the chondrocytes are round and densely packed. The water content is its lowest and the proteoglycan content at its highest in this zone. Finally, the calcified cartilage (below the tidemark) links the cartilage to the subchondral bone. Hypertrophic chondrocytes are found in the calcified zone [25, 28, 129, 148].

The thickness of adult human cartilage typically varies between 2–5 mm, the thickness of the calcified cartilage and the subchondral plate in adult humans is ≈ 0.13 mm and ≈ 0.19 mm, respectively [82]. Furthermore, the structural architecture of articular cartilage is created by a synchronized process of tissue resorption and neoformation [81].

Table 2.1: Structure and content from the main components of articular cartilage [129] ($\downarrow$ decrease, $\uparrow$ increase).

	water	collagen	proteoglycan
wet weight	60–85%	15–22%	4–7%
dry weight	–	50–80%	5–10%
diameter	–	20–200nm	–
length	–	–	$10^{-8} - 10^{-6}$m
content in zones			
surface			
$\updownarrow$	$\downarrow$	$\downarrow$	$\uparrow$
deep			

Table 2.2: Macromolecular interactions in articular cartilage [129].

	collagen–collagen	**PG–PG**	**collagen–PG**
Type	• covalent cross-link	• Repulsive forces between negatively charged GAGs	• non-covalent bonding 1) electrostatical 2) mechanical
Function	collagen network • stiffness • strength	• compressive stiffness • Donnan osmotic pressure • retaining the molecules on the tissue	• PGs(-) interacting with collagen (+) • hyaluronates from aggregates interacts with collagen II • swelling pressure

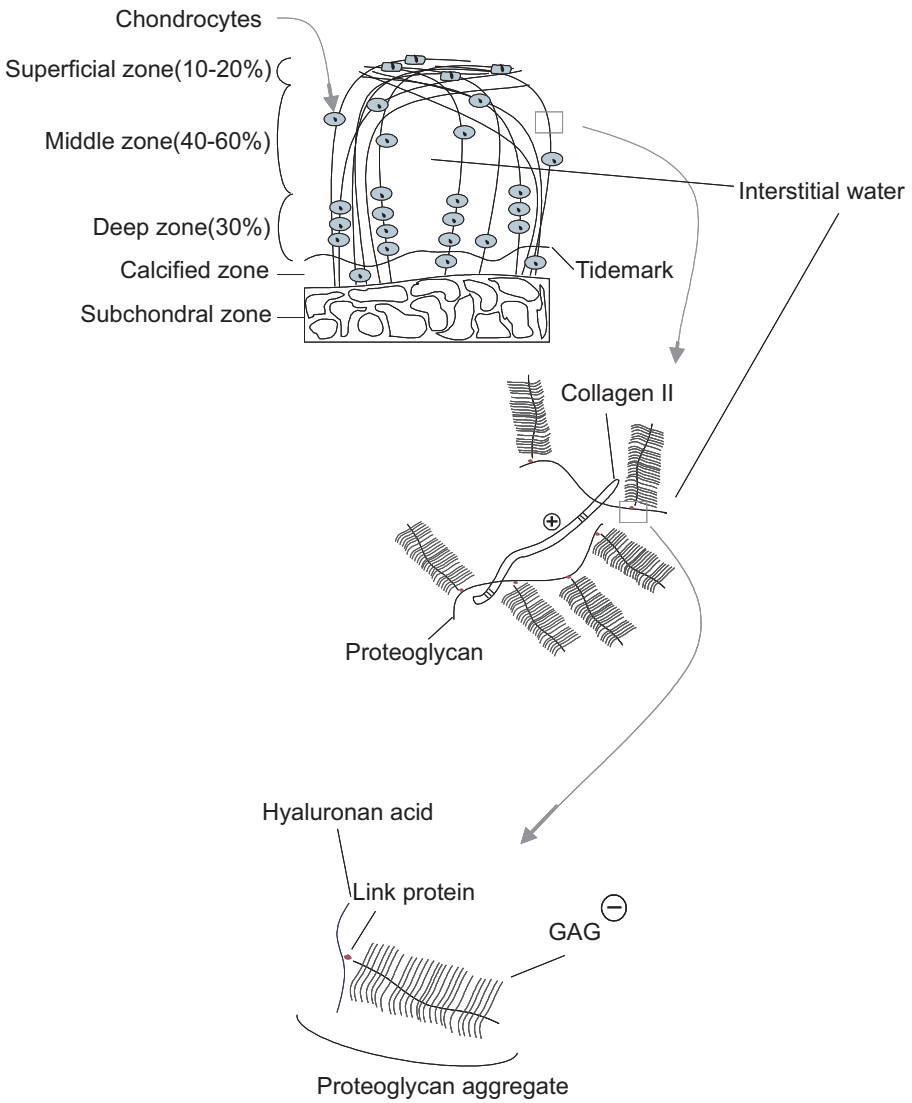

Figure 2.1: Structure of articular cartilage.

2.2 Mechanical properties of articular cartilage

Cartilage is an inhomogeneous, poroelastic material with nonlinear mechanical properties. The mechanical properties vary between species [8, 166], cartilage layers [186] and anatomical locations [86, 110]. Furthermore, the measurement direction affects the mechanical response, *i.e.* the mechanical properties are anisotropic [96]. The mechanical properties can be determined from the load–deformation behavior of the tissue. When

the cartilage is loaded, flow of the interstitial fluid through the extracellular matrix creates a poroviscoelastic response. When the load is removed, the tissue restores its thickness and shape by resorption of the fluid. There is no fluid flow at mechanical *equilibrium*, and the load is controlled by the solid matrix. During *instantaneous loading*, elastic deformation without interstitial fluid flow takes place.

It has been shown that the collagen network is mainly responsible for the dynamic response under compression [98, 129], whereas PGs are responsible for the static compressive stiffness of cartilage [95, 129]. Due to tissue complexity, the nonlinear behavior of articular cartilage is most often numerically modeled by using finite–element analysis [46, 194].

Unconfined compression, *confined compression* and *indentation* measurements are used to study experimentally the mechanical properties of articular cartilage. Further, three experimental loading techniques are traditionally used: *stress–relaxation*, *creep* and *dynamic loading* (figure 2.2). In *unconfined compression*, cartilage without the subchondral bone is compressed between two smooth and rigid plates, and fluid flows only in the lateral direction. The stiff collagen structure in the superficial tissue allows a lesser lateral expansion as compared to the deeper parts of the cartilage. In *confined compression*, a sample with or without bone is placed in a rigid chamber and compressed with a porous filter. Fluid can only flow axially through the tissue surface into the filter. Under unloaded state, the swelling of PGs is limited by the elastic forces of the collagen network [121]. In the axial direction, compressive stiffness increases [186] and tensile stress decreases [2] towards the deep cartilage. Unconfined and confined compression measurements can be conducted only in the *in vitro* setting.

In unconfined compression, at equilibrium, Young's modulus of isotropic elastic material is given by

$$E_{eq} = \frac{\sigma}{\epsilon}, \tag{2.1}$$

where σ is axial stress and ϵ is axial strain in the solid matrix. In confined compression, the equilibrium modulus is called the aggregate modulus H_A, related to E and ν:

$$H_A = \frac{(1-\nu)}{(1+\nu)(1-2\nu)}E, \tag{2.2}$$

where E is Young's modulus and ν is Poisson's ratio. The complex dy-

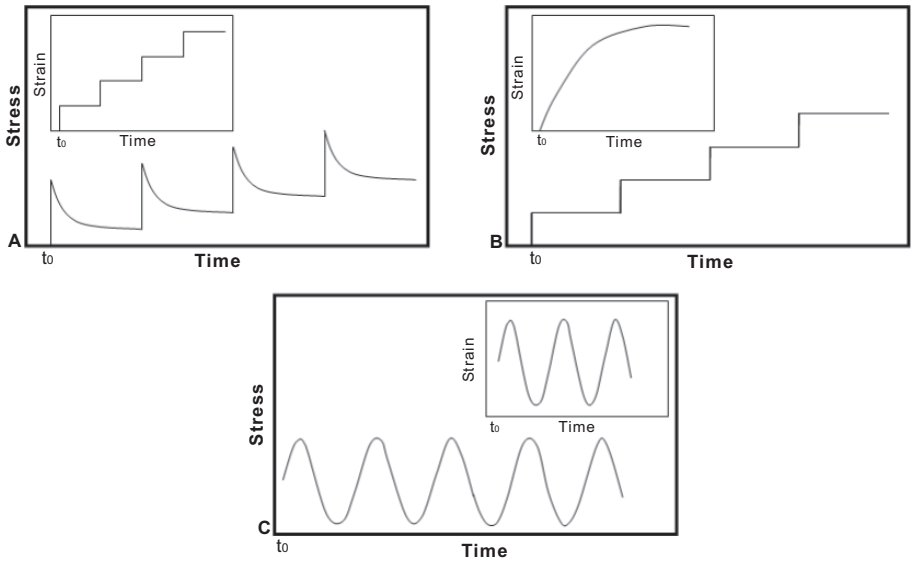

Figure 2.2: (A) In a stress-relaxation experiment, the load (stress) is measured under a constant deformation (strain). (B) In a creep experiment, cartilage deformation (strain) is measured under constant load (stress). (C) In a dynamic loading experiment, the response of the tissue to cyclic deformation is measured.

namic modulus of cartilage is given by

$$|G_d| = \sqrt{G_1^2 + G_2^2} = \frac{\sigma_d}{\epsilon}, \tag{2.3}$$

where σ_d is the dynamic stress, G_1 the storage modulus, proportional to the elastically stored energy, and G_2 is the loss modulus, *i.e.* the viscous energy lost in the loading process.

Indentation measurements can be conducted both *in vitro* and *in vivo*. Cartilage is compressed using an indenter, leading to fluid flow, both in axial and lateral directions. In this geometry, the thickness of the superficial zone and the transverse stiffness both play important roles in determining the mechanical response [97].

Typical values for Young's modulus or aggregate modulus of the intact articular cartilage are 0.2–1.5 MPa [4, 7, 30, 36, 86, 90, 96, 98, 129, 196]. Poisson's ratio varies between 0.00–0.43 [8, 36, 87, 96] and values for instantaneous or dynamic ($t \to 0$) modulus are around 1.5–20 MPa [30, 52, 98, 103, 149]. The values depend significantly on the species and the anatomical location of the tissue [8, 86, 110, 166].

Several theoretical models have been devised to predict the mechanical behavior of cartilage. Finite–element analysis (FE) offers the most realistic model for the nonlinear behaviour of articular cartilage. A *single phasic elastic model* assumes the material to be inhomogenous and elastic with constant mechanical properties, *i.e.* isotropic elastic material with uniform mechanical properties in all directions. In this model, only Young's modulus and Poisson's ratio are required to characterize the mechanical behavior of the material [75]. However, the complex nonlinear behavior of cartilage, structural and mechanical anisotropy make the modeling more challenging. The single phasic model is not very realistic, as cartilage consists of two phases.

The *biphasic model* includes the two phases of cartilage, *i.e.* solid and fluid. This is a more realistic presentation of cartilage since the motion of the interstitial fluid has a major impact on the viscoelastic behavior of articular cartilage. The *linear isotropic biphasic model* assumes the solid and fluid phases to be incompressible, the solid matrix being isotropic, homogenous and porous whereas the fluid phase is inviscid [128]. This is the most traditional model for characteristing the mechanical behaviour of articular cartilage. However, it fails to predict tensile behaviour [98] or short–term compressive behaviour in unconfined compression [37].

The *transversely isotropic model* takes into account the dynamic response better than the isotropic biphasic model [97]. This model can utilize one [195] to two [32] permeability coefficients and five elastic constants. Even though this model includes the parallel oriented collagen fibers in the superficial cartilage layer, it still fails to predict the compression–tension nonlinearity of the tissue.

In the *fibril-reinforced poroelastic model*, the role of the collagen fibers is considered to provide the stiffness in tension only. This takes into account the compression–tension nonlinearity and time–dependent deformation of the intrinsic viscoelastic matrix [112]. A biphasic model, where an ion phase is included, is called the *triphasic model* [171]. This includes tissue swelling, and in this model the stress, strain, ion concentrations, electric fields and flow fields can be defined [68–70].

2.3 Osteoarthritis

Osteoarthritis (OA) is a degenerative joint disease that in its more severe form disrupts the extracellular matrix. Mainly, it appears in patients over the age of 50 years, with the majority being women. In Finland, the 'Health 2000' study revealed that 16% of men and 32% of women are suffering from knee arthrosis at the age of 75–84 years [6]. In the United States,

approximately 135 000 procedures are done yearly to repair knee defects or to undertake total knee replacements [24]. Thus, OA is a significant health and economic burden to our society [199].

Cartilage has a poor spontaneous capacity to heal itself after an injury or disease [27]. The early stages of OA are often asymptomatic but later the clinical symptoms of OA include limitations of joint movements, deformation and effusion of the joint, pain and abnormal sounds from the joint (*i.e.* crepitation with motion). OA can be initiated by an injury, or it may arise after infection (*i.e.* osteoarthritis) or after metabolic and neurological disorders. OA can also occur spontaneously without any obvious reasons [27].

The earliest symptoms of OA, characteristics of *early degeneration*, include fibrillation of the collagen fibers, which starts on the articular surface and proceeds to the middle zone. There is also loss of PG aggregans, tidemark damage, the appearance of blood vessels from the subchondral bone and subchondral bone modifications [10, 25]. In X–ray images, the first sign are ostephytes. These changes lead to an increase in tissue permeability, water content and swelling of cartilage [113]. Concomitantly, the mechanical stiffness of articular cartilage becomes reduced. Nonetheless, this stage is normally asymptomatic for the individual, the cartilage surface seems still regularly glossy and no damage on the surface may be seen. Later, in *advanced degeneration*, due the changes in osmolarity and ionic charge, chondrocytes release mediators, stimulating metabolic response of cells, aiming to heal the cartilage. An expansion of aggregates and an increase in the water content occurs in the cartilage tissue and also the density of subchondral bone increases. At this stage, changes in glossiness and in the color of the cartilage surface may become apparent. Deep defects down to the subchondral bone can be seen [27]. In the third and final stage of OA, *late degeneration*, cartilage is fully destroyed, leaving only the thickened and dense subchondral bone for joint contact. The shape of the joint may change and other clinical symptoms, *i.e.* limping, pain, joint deformity and instability are typically encountered. The loss of cartilage leads to secondary changes in synovial tissue, ligaments, capsules, and joint muscles [27]. Decreased range of motion and muscle atrophy follow after reduced use of the joint.

The diagnostics of OA is usually carried out with X–ray imaging where joint space narrowing, subchondral bone sclerosis, cysts and ostephytes, *i.e.* typical symptoms of degenerated cartilage, can be observed. Unfortunately, the early stage of OA cannot been detected by X–ray evaluation. Another common diagnostic method is arthroscopic examination. One major prolem of arthroscopy is its invasive nature. Furthermore, it is a

subjective examination and depends critically on the individual who performs the examination [23]. Although surface fibrillation and the general condition of the joint can be visually detected, the internal cartilage structure and modifications of the subchondral bone cannot be diagnosed.

Magnetic resonance imaging (MRI) is a widely used non–invasive method to examine articular cartilage [62, 126]. The water content of the normal healthy articular cartilage tissue is 60-85% [129]. Since the early OA changes include an increase of the cartilage water content, MRI represents a potential method to detect the early stage of OA. Alterations on the subchondral bone may also be diagnosed [44, 190].

2.4 Cartilage repair

The only treatment for advanced osteoarthritis is prosthetic joint replacement. However, several methods have been introduced to attempt treatment of locally damaged cartilage. Unfortunately, none of these methods have been shown to produce hyaline tissue with a similar composition, structure or mechanical properties as native articular cartilage.

Drilling of the subchondral bone plate to stimulate the cells from the bone marrow to transform them into cartilage cells, was the first cartilage repair technique in humans which achieved satisfactory results [42]. Later, the drilling was changed to *microfracture technique*, which today is the most common technique in use to repair cartilage lesions [27, 169]. *Mosaicplasty* is a technique that has been introduced for smaller osteochondral defects [72, 73]. In mosaicplasty, osteochondral plugs are taken from the less weight-bearing peripheral joint surface and transferred to the corresponding holes in the lesion site. In the space between the plugs, fibrous cartilage takes place. *Fresh osteochondral allografts* can be used to replace large areas of bone and cartilage, and their use is the recommended treatment for young, active patients with large, traumatic osteochondral defects [67]. These grafts are difficult to obtain, which limits their use. More than ten years ago, *soft tissue grafts*, such as periosteal or perichondrial grafts were under intensive examination, but the results have been disappointing, and they are not in widespread clinical use [78, 139, 154]. *Cell transplantations* were introduced after the observation that the chondrocytes around the lesion were not able to move into the repaired area. Therefore, it was necessary to bring extra cells to produce matrix in the damaged area. Earlier, cultured autologous chondrocytes have been succesfully isolated and transplanted in cartilage defects in rabbits [61].

The method most closely studied in this thesis work, *autologous chondrocyte transplantation* (ACT) (also known as Autologous Chondrocyte Im-

plantation (ACI)), was first used in human patients by Brittberg *et al.*[24]. In the study of Brittberg *et al.*, a total of 23 patients with deep cartilage defects underwent ACT surgery, where autologous chondrocytes were cultured under laboratory conditions and injected into the cartilage lesion, covered with a periosteal flap. Three years (36 months) after the operation, 15 out of 16 femoral transplants and 1 out of 7 patellar transplants showed the appearance of hyaline cartilage. Subsequently, ACT has been studied and is now widely accepted as a beneficial cartilage repair technique [57, 119, 146, 147, 157, 184]. It is noted that chondrocytes can produce collagen type II in cell cultures, and biopsies have revealed hyaline–like cartilage or hyaline–fibrous cartilage in cartilage grafts [11, 76, 155].

CHAPTER III

MRI of articular cartilage

3.1 Nuclear magnetic resonance (NMR)

Nuclear magnetic resonance (NMR) is based on the interaction of a magnetic nucleus and its spin s with an external magnetic field, B_0. The focus in this work is on hydrogen (^{1}H), also referred to as the proton (since hydrogen nuclei contains a single proton). The spin of the nucleus is nonzero when the number of protons Z and/or the number on neutrons is odd.

The magnetic dipole moment, μ, has the direction of the B_0 field, giving the direction for the spinning motion of the nuclei. The nucleus can have $2s + 1$ energy stages:

$$E = -m_s \gamma \hbar B_0 = -m_s \hbar \omega_0, \tag{3.1}$$

where m_s=$-s$, $-s + 1$, ..., $s - 1$, s and $\hbar$ is Dirac's constant. ^{1}H has two possible energy levels: parallel ($+1/2$) or anti-parallel ($-1/2$) state with respect to the static field. The uneven distribution of the proton populations is given by the Bolzmann equation

$$\frac{N_{-1/2}}{N_{+1/2}} = e^{-\Delta E/kT} = e^{-\hbar\omega_0/kT}, \tag{3.2}$$

where N is the number of nuclei in the spin orientation, ΔE is the energy difference between the states, T is the temperature and k is Boltzmann's constant (1.38x10$^{-23}J/K$). As the spin of the hydrogen nucleus is ($\pm 1/2$), it has only one quantized energy describing the transition between the states. Since there is a large number of a hydrogen nuclei in biological tissues, this is a perfect match for biological and medical MR applications. This large number of hydrogen nuclei in the tissue gives rise to the net magnetization M_0 along the B_0.

In a static B_0 field, nuclei will precess in the direction of the magnetic field at Larmor frequency given by

$$\omega_0 = \gamma B_0, \tag{3.3}$$

where γ is a constant called the gyromagnetic ratio. For example, in water, the hydrogen proton has a value of γ=2.68x10^8 $rad/s/T$ or 42.6 MHz/T).

3.2 Relaxation

An additional quantum of energy can change the direction of the spin state of the nucleus away from the direction of the z–axis, provided that it is introduced with a frequency matching the Larmor frequency of the given nuclei. This is called a rf–pulse that induces a magnetic field, B_1. Applying B_1 for a duration t will tilt the net magnetization $90\,^\circ$ ($\pi/2$ pulse), *i.e.* into the xy–plane, leading to zero magnetization in the direction of the z axis. A pulse at the same power but duration $2t$ will rotate the magnetization by $180\,^\circ$ (π pulse), *i.e.* it will invert the orientation of spin populations. The field in the xy–plane is described as

$$\overline{B_1} = B_1(cos\omega_0 t\hat{x} - sin\omega_0 t\hat{y}), \tag{3.4}$$

inducing a time dependent behaviour of the net magnetization:

$$\frac{dM}{dt} = \gamma\overline{M} \times \overline{B_{ext}}, \tag{3.5}$$

where $\overline{B_{ext}} = \overline{B_0} + \overline{B_1}$. The different components of M are given as

$$\frac{dM_x}{dt} = \gamma(M_y B_0 + M_z B_1 \sin\omega_0 t), \tag{3.6}$$

$$\frac{dM_y}{dt} = \gamma(M_z B_1 \cos\omega_0 t - M_x B_0), \tag{3.7}$$

$$\frac{dM_z}{dt} = \gamma(M_x B_1 \sin\omega_0 t + M_y B_1 \cos\omega_0 t). \tag{3.8}$$

After the rf–pulse, the excited spins will immediately start to arrange towards the equilibrium, a phenomenon called relaxation. The change in magnetization induces a current into the rf coil, producing a signal known as the free induction decay (FID). Since this is time dependent, the frequency distribution can be revealed using Fourier transform (FT). The recovery of magnetization is represented by the Bloch equations [19]

$$\frac{dM_{xy}}{dt} = -\frac{M_{xy}}{T_2}, \tag{3.9}$$

$$\frac{dM_z}{dt} = \frac{M_0 - M_z}{T_1}. \tag{3.10}$$

The recovery in the z–axis direction is called longitudinal or spin–lattice relaxation, T_1, and the decay in the xy–plane is called transversal or spin–spin relaxation, T_2.

3.2.1 Spin–lattice relaxation (T_1)

Protons are in thermal contact with the lattice of their nearby atoms, and each proton will experience different magnetic field variations. In addition, the local magnetic fields created by rotation, translation and vibration of these atoms affect the field variations. After the 90° rf–pulse, the longitudinal magnetization evolves in an exponential manner, until the z–component of net magnetization is recovered. This can be derived from equation 3.10:

$$M_z(t) = M_z(0)e^{-t/T_1} + M_0(1 - e^{-t/T_1}). \tag{3.11}$$

The relaxation occurs when a component of the fluctuation frequency matches the nuclear Larmor frequency and stimulates a spin flip. The rate of field fluctuations is characterized by the *correlation time* τ_c. The relationship between T_1 relaxation rate and the frequency distribution of the molecular motion can be described as [26, 54]:

$$\frac{1}{T_1} \propto B_{xy}^2 \frac{\tau_c}{1 + \omega_0^2 \tau_c^2}, \tag{3.12}$$

where ω_0=2πf_0 is the resonance frequency. The relaxation is most efficient when τ_c=1/ω_0.

Inversion recovery is a technique for producing T_1contrast, consisting of a combination of two rf–pulses. First, a π–pulse is introduced which inverts the equilibrium magnetization. Longitudinal magnetization now starts to increase and no transversal magnetization is created. The net magnetization vector will eventually return back to +z axis at a rate determined by T_1. Since the magnetization on z axis is not detectable, a $\pi/2$–pulse is introduced to tip the longitudinal magnetization back to the xy–plane. Following the $\pi/2$–pulse, the signal is given as [71]

$$M_z(TI) = 0 \tag{3.13}$$

$$M_{xy}(TI) = M_0(1 - 2e^{-TI/T_1}), \tag{3.14}$$

where TI is the time between the inversion pulse and the 90–degree pulse, *i.e. inversion time*, and M_0 is the net magnetization. The selection of TI

defines the amount of T_1–weighting in the registered signal. When this experiment is repeated with several TI values, T_1 can be determined using equation 3.14. The factor 2 in equation 3.14 assumes that the magnetization is at full inversion. This factor can also be fitted to account for inaccuracies in the inversion.

Previously, native T_1 relaxation time of cartilage has been shown to correlate with biomechanical parameters, degeneration stage, proteoglycan depletion [99, 135, 138, 175, 183] and T_1–weighted imaging has been used to evaluate repaired cartilage and cartilage lesions [35, 48, 49, 188]. In addition, T_1 has been claimed to be able to monitor the biophysical properties of engineered cartilage [120]. However, the relationship between T_1 and cartilage composition is not fully understood. It has been reported to be relatively constant throughout the tissue depths [122, 197], and to be isotropic, *i.e.* showing no orientational dependence [77].

3.2.2 Spin–spin relaxation (T_2)

In addition to the applied field, spins experience differences in the local field due to their mutual presence. This leads to different local precession frequencies. Energy exchange with the lattice is not involved. Due to the variations on the local magnetic field, the individual magnetic moments will gradually lose their phase coherence, leading to a dephasing of the net magnetization vector. This leads to a signal decay, known as spin–spin relaxation. Solving the equation 3.9, transverse relaxation is given by

$$M_{xy}(t) = M_{xy}(0)e^{-t/T_2}. \tag{3.15}$$

The relationship between the relaxation rate $1/T_2$ ($= R_2$) and spectral density is described as

$$\frac{1}{T_2} \propto B_z^2 \tau_c. \tag{3.16}$$

As well as the dephasing of individual spins, there is also additional dephasing caused by field inhomogeneities. The total relaxation time (T_2^*) is a consequence of these terms given by

$$\frac{1}{T_2^*} = \frac{1}{T_2} + \frac{1}{T_2'}, \tag{3.17}$$

where T_2' is the transverse relaxation due to the presence of field homogeneities causing a signal decay. This can be compensated with a method called the *spin echo* technique. This contains two rf–pulses, a $\pi/2$–pulse followed by a refocusing π–pulse. The first pulse tips the magnetization

into the xy–plane and the spins begin to dephase. After a time τ, a second pulse reverses the spins in such a way that the spins earlier experiencing a positive phase now experience a negative phase, and *vice versa*. After the π–pulse, the spins begin to rephase creating an echo. The time from the $90\,^\circ$ pulse to the maximum intensity of the spin–echo is called the *echo time*, TE=2τ. The detected magnetization is given by

$$M_{xy}(TE) = M_{xy}(0)e^{-TE/T_2}. \tag{3.18}$$

The T_2 relaxation time constant can then be determined from the signal intensity measurements with variable TE–times. When only one refocusing pulse is applied after excitation, the experiment is called a *single echo spin echo* sequence.

Rubenstein *et al.* reported the strong orientation dependence of T_2–weighted imaging in cartilage due to the oriented collagen structure [158]. Subsequently, T_2–weighted imaging has been often used to visualize the network arrangement within the cartilage layers, due to the magic angle effect [59, 65, 134, 198]. Depending on the cartilage orientation in B_0, the dipolar interaction within zones become altered, thus affecting T_2. This interaction is at its minimum at $54.7\,^\circ$, *i.e.* at the magic angle. This appears with high signal intensity in T_2–weighted images.

T_2 imaging has been used in knee MRI studies, concerning cartilage lesions where T_2 values of the focal cartilage defects were found to be higher than values in the adjacent cartilage [102]. Osteoarthritis studies noted that T_2 mapping of articular cartilage may reveal early cartilage lesions not visible with standard clinical MRI and may be useful in quantifying early OA related changes [74, 167]. ACT cartilage repair techniques have been studied with T_2 relaxation time by White *et al.* [193]. They showed that qualitative and quantitative T_2 mapping helped to differentiate hyaline cartilage from reparative fibrocartilage after cartilage repair. T_2–weighted imaging was reported to be unable to predict ACI graft histological features [174], whereas another study claims MRI to be a useful non–invasive tool for evaluating the morphologic status of osteochondral plug transfers [182].

Proton density or T_2 relaxation time measurements have also been speculated to reflect the water content in the tissue [106, 109, 162]. T_2 has also been proposed to depend on the level of PGs [150, 189]. T_2 has been related to the mechanical properties of articular cartilage, since it revealed a significant correlation with Young's modulus and dynamic modulus [99, 135, 138, 189]. T_2 imaging has been also shown to be able to differentiate degeneration [138, 141], maturity [140], morphology [200] and topographical variations [135, 187] of cartilage samples.

3.3 dGEMRIC

A contrast medium that is frequently used in MRI is a gadolinium complex with diethylenetriamine pentaacetic acid (Gd-DTPA^{2-}), supplied in the form of dimethylglucamine salt. Free Gd^{3+} is very rare and toxic, and therefore it is necessary to bind it with a high stability constant chelate. The gadolinium atom carries seven unpaired electrons and hence is strongly paramagnetic, shortening the relaxation times [47]. Other important paramagnetic ions are chromium (Cr^{2+}), manganese (Mn^{2+} and Mn^{3+}) and iron (Fe^{2+}), often embedded in chelates when used in MR studies. The contrast agent concentration can be presented as

$$[Gd - DTPA^{2-}] = \frac{1}{R}(\frac{1}{T_{1Gd}} - \frac{1}{T_1}), \tag{3.19}$$

where R is the relaxivity of Gd–DTPA in ($mM^{-1}s^{-1)}$), often expected to be the value of saline solution [38], T_1 and $T_{1\mathrm{Gd}}$ are the relaxation times without and with the contrast agent, respectively.

Bashir *et al.* measured the human cartilage GAG concentration with the gadolinium enhanced MRI of articular cartilage (dGEMRIC) technique [13, 14]. Since GAGs have negatively charged side groups, Gd-DTPA^{2-} ions will be distributed in cartilage, reflecting the local GAG concentration, with higher concentrations in those areas with depleted GAGs and *vice versa*. The spatial contrast agent concentration is inversely related to GAGs, the main source of tissue FCD. Bashir *et al.* noted the connection between Gd-DTPA^{2-} and FCD [13, 14]:

$$FCD = 2[Na^+]_b(\sqrt{\frac{[Gd - DTPA^{2-}]_t}{[Gd - DTPA^{2-}]_b}} - \sqrt{\frac{[Gd - DTPA^{2-}]_b}{[Gd - DTPA^{2-}]_t}}), \tag{3.20}$$

where t and b refer to tissue and bath, respectively.

The relaxivity differs between tissues and magnetic field strengths [38, 165]. The $T_{1\mathrm{Gd}}$ relaxation time is related approximately linearly with the GAG content of cartilage [13, 14]. Subsequently, dGEMRIC became a widely accepted and used method to measure cartilage GAGs *in vivo* [12, 107, 115, 156, 173, 179] and *in vitro* [9, 99, 125, 133, 179]. dGEMRIC has been shown to predict the compressive stiffness of articular cartilage *in vitro* [99, 135, 138, 159, 189]. Protocol issues have been published [29] and the technique has been used to evaluate the healing process and GAG content in ACT patients [55, 184]. The sensitivity of the dGEMRIC technique has been shown to be good in hip dysplasia and in OA studies it can identify poor candidates for a pelvic osteotomy and dGEMRIC values have correlated with pain and the severity of the dysplasia [33, 91, 172].

Limitation in the accuracy of the dGEMRIC method was raised in a study where relaxivity was shown to be dependent on the macromolecular content [168]. However, cartilage was not studied.

Recently, Nieminen *et al.* suggested that it might be possible to combine the imaging sessions from T_2 and dGEMRIC [132]. Until now T_2 and dGEMRIC are being imaged in separate imaging sessions since Gd-DTPA^{2-} may affect native T_2 by offering an additional relaxation mechanism. The effect of Gd-DTPA^{2-} was greater with high concentration and long T_2s while the deep tissue which have relatively low T_2s and [Gd-DTPA^{2-}] values was not significantly altered by Gd-DTPA^{2-} [132]. Finally, it has been shown that it is possible to obtain accurate morphological measurements of cartilage in the presence of Gd-DTPA^{2-} and that morphological and dGEMRIC measurements may be combined in a single imaging session [43].

3.4 Other quantitative MRI methods

Spin–lattice relaxation in the rotating frame, $T_{1\rho}$ relaxation, provides information about macromolecules with slow rotational motions. In this spin–lock method, spins are 'locked' in the xy–plane by applying a continuous rf–pulse. Magnetic moments are then precessed around the spin–lock field. During a spin–lock pulse, the magnetization relaxes towards equilibrium with the relaxation constant $T_{1\rho}$. $T_{1\rho}$ has been found to be sensitive to the cartilage PGs [1, 40, 41, 105, 144, 151, 152]. Relaxation mechanisms in the rotating frame in cartilage have also been investigated, revealing that $T_{1\rho}$ is also dependent on the collagen orientation of the cartilage due to residual dipolar coupling [124].

Magnetization transfer, MT, involves the exchange of magnetization between bound (*i.e.* immobilized or adsorbed) water and protein protons. In a MT experiment, a long rf pulse is applied at the off–resonance frequency from the bulk water resonance, saturating the proton magnetization. When the components (*i.e.* water or protein protons) are saturated, the exchange of magnetization occurs until a steady state is achieved. A reduction of the signal intensity of the bulk water is then observed. In cartilage, collagen plays the main role in MT, since PGs make only a minor contribution to MT [63, 100, 101, 160, 185].

Diffusion is the random motion of the water molecules in the tissue. *Diffusion tensor imaging* (DTI) experiment is done by applying diffusion–-sensitizing gradients and registering diffusion–related signal attenuation. The self–diffusion of the water protons characterised by a 3x3 tensor, describing both the magnitude and the direction of the diffusion in a 3–

dimensional space [15]. It has been shown that the DTI method can be used to measure diffusion anisotropy in human cartilage and that the direction of the maximum diffusion reflects the alignment of collagen fibers, *i.e.* motional anisotropy of water is a consequence of the attraction or binding water molecules by collagen [50]. Diffusion constants may also reflect structural degradation of the cartilage matrix. *Apparent diffusion constant* (ADC) has been shown to be sensitive to proteoglycan depletion [175] and may reflect the structural degradation of the cartilage matrix [123]. DTI has been studied in enzymatically degenerated bovine [116] and human [34] cartilage, indicating that GAG loss slightly increases the diffusion anisotropy and the ADC in the cartilage. However, no changes were noted in fractional anisotropy [34, 116].

The negatively charged side groups of GAGs attract sodium ions around them, assuring electroneutrality in the tissue. The early stage of OA is primarily associated with a loss of PGs, which leads to a decrease in the sodium concentration. Based on this, sodium has been used to reflect the PG depletion in the cartilage [21, 31, 108]. Shapiro *et al.* showed that sodium assessed accurately the FCD in articular cartilage [161]. Sodium MR imaging has also shown to represent a potential method for use as a quantitative diagnostic tool to measure changes in proteoglycan content in early-stage osteoarthritis [192].

Collagen fibers attract water molecules by inducing motional anisotropy. The signal of these water molecules can be effectively detected by the ^{2}H spectroscopic imaging technique that is based on the distribution of the ^{2}H quadrupolar splitting and further the spatial orientation of collagen fibers [88, 131, 163]. ^{2}H spectroscopic imaging has been shown to be sensitive to the order and density of the collagen fibers in pig articular cartilage from birth to maturity [89]. The effect of load applied to the cartilage-bone plug has been monitored and the orientation and the degree of order of the collagen fibers at each spatial location on a cartilage plug has been estimated [164].

Since thinning in cartilage thickness is involved in OA, *in vivo* cartilage thickness and volume have been a subject of interest for clinicians. Females with a higher incidence of knee osteoarthritis (OA) than males have thinner cartilage and smaller joint surfaces, even after adjustment for height and body weight [142]. Nonetheless, it has been shown that thin cartilage does not predispose to OA [80]. In addition, the factors stimulating bone and cartilage growth may differ between the sexes [143]. The fat suppression gradient echo imaging offers the possibility to study cartilage morphometry. Building three–dimensional virtual computer presentations, it is possible to improve accuracy compared with two–dimensional

plane images [20, 22, 44, 45, 47, 56, 94, 104]. 3D imaging has also been successfully used to shorten the examination time in articular cartilage imaging [176], for monitoring the healing process of the lesion after surgical cartilage repair [178] and, together with dGEMRIC, to evaluate the relative glycosaminoglycan content of repair tissue after matrix–associated autologous chondrocyte transplantation (MACT) [178, 180], which is a three–dimensional biomaterial scaffold used as a carrier for chondrocytes. 3D imaging has also been used successfully in a fast semi–automated software method to segment the cartilage in knee MRI [39]. 3D MRI was shown to measure accurately and reliably small changes in cartilage volume *ex vivo* [85].

Normal tendons, ligaments and uncalcified fibrocartilage produce little or no signal and they appear dark with all pulse sequences caused by their short T_2s. With ultrashort TE (UTE), it is possible to identify in a specific manner, the calcified cartilage and uncalcified fibrocartilage [16, 181].

CHAPTER IV

Aims of the present study

Several quantitative magnetic resonance imaging techniques, based on ^{1}H NMR relaxation properties, have been developed for the characterization of structure and composition of articular cartilage. The present study has applied qMRI techniques in an attempt to elucidate variations in properties of native and repaired cartilage in the animal and human joint, and in this way to evaluate the clinical applicability of quantitative MRI techniques. The aims of the present *in vitro* and *in vivo* studies were

1. to study the topographical variations of the cartilage MRI properties in the human knee joint and to relate T_2 relaxation time and dGEMRIC imaging techniques with the structural and biomechanical properties of human cartilage;

2. to study whether T_2 and dGEMRIC imaging techniques can be merged into one imaging session and be able to produce reliable quantitative information on the collagen structure of cartilage using T_2 relaxation time measurements in the presence of Gd-DTPA^{2-};

3. to study whether native T_1 relaxation time could serve as a biomarker to characterize the water content of articular cartilage;

4. to investigate the importance of combining T_2 relaxation time and dGEMRIC techniques to monitor the regeneration of cartilage tissue after ACT surgery.

CHAPTER V

Materials and methods

The present thesis consists of four independent studies (I-IV), three *in vitro* studies with cadaver human or bovine samples and one *in vivo* study in ACT patients. A summary of the methods used is presented in table 5.1.

5.1 *In vitro* experiments

5.1.1 Sample preparation

CADAVER HUMAN SAMPLES

In studies I and II, left knees of human cadavers (n = 13, age 20–80 years) were obtained from Jyväskylä Central Hospital, Jyväskylä, Finland, with permission from the national authority (National Authority of Medicolegal Affairs, Helsinki, Finland, permission 1781/32/200/01). Knees were frozen post–mortem and, after thawing, full–thickness cartilage–bone cylinders (diameter = 16 mm, n = 78) with subchondral bone were drilled from nonarthritic knees at six anatomical locations: the latero–proximal patella (PAT), medial/lateral condyles of the femur (FMC/FLC), medial/-lateral tibial plateaus (TMP/TLP) and the femoral groove (FG) (figure 5.1). One patellar sample was excluded because of cartilage degeneration. The samples (n = 77) were frozen at $-20\,^{\circ}\mathrm{C}$ after immersing them in phosphate–buffered saline (PBS; Euroclone Ltd., Paignton–Devon, UK) containing enzyme inhibitors (5 mM ethylenediaminetetraacetic acid (EDTA) (Merck, Damstadt, Germany) and 5 mM benzamidine HCl (Sigma, St. Louis, MO)). Before the measurements, the osteochondral plugs were thawed, and smaller full–thickness cartilage disks (diameter = 4.0 mm) without subchondral bone were prepared with the use of a biopsy punch and a razor blade. Six anatomical sites were included in study I, whereas in study II knees without patellar samples were examined (n = 65).

Table 5.1: Materials and methods used in studies I–IV. All cartilage samples exhibited non–arthritic tissue. In studies I–II, samples were cadaver human cartilage, in study II, a part of the measurements and the whole study III were done with intact bovine articular cartilage. Study IV was performed *in vivo*.

Study	Samples	Methods	Parameters
I	Cadaver human samples (n=77) from: PAT ($n = 12$), FMC ($n = 13$), FLC ($n = 13$), TMP ($n = 13$), TLP ($n = 13$), FG ($n = 13$)	Magnetic resonance imaging Biomechanical testing	T_2, T_1, $T_{1\mathrm{Gd}}$, $[Gd]$ E_{eq}, G_d
II	Cadaver human cartilage ($n = 65$) from: FMC ($n = 13$), FLC ($n = 13$), TMP ($n = 13$), TLP ($n = 13$), FG ($n = 13$) Bovine cartilage (PAT, $n = 4$)	Magnetic resonance imaging Polarized light microscopy	T_2, $T_{2\mathrm{Gd}}$, $T_{1\mathrm{Gd}}$ BF
III	Bovine cartilage samples ($n = 20$) from: PAT ($n = 8$), FMC ($n = 4$), TMP ($n = 4$), LPG ($n = 4$)	Magnetic resonance imaging Optical density measurements Biochemical analysis	T_1, T_2 PG H_2O
IV	ACT patients ($n = 13$) having lesions at FMC ($n = 6$), FLC ($n = 3$), Throclea ($n = 4$)	Magnetic resonance imaging	PD, T_2, $T_{1\mathrm{Gd}}$

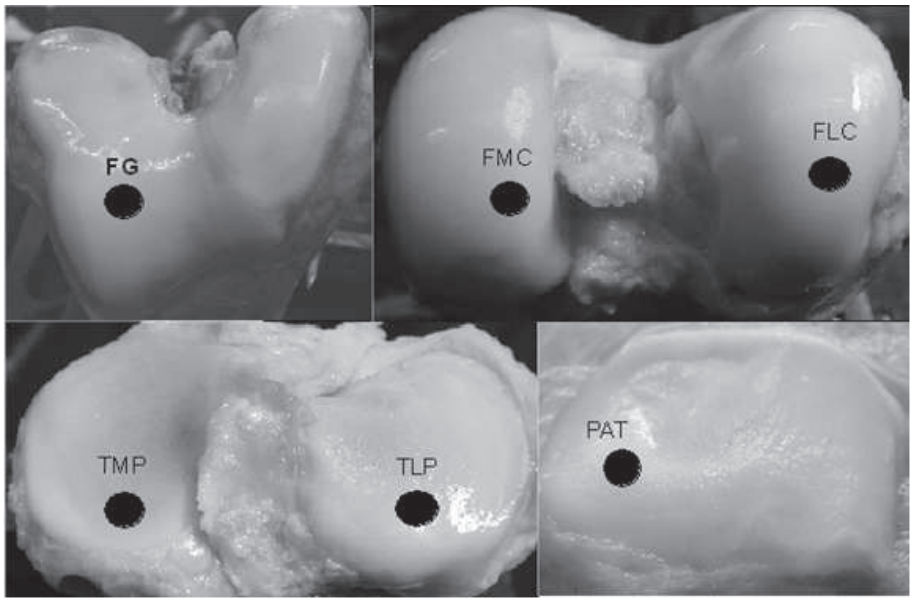

Figure 5.1: Articular cartilage samples from different anatomical locations: femoral groove (FG), medial/lateral condyles of the femur (FMC/FLC), medial/lateral tibial plateaus (TMP/TLP) and latero–proximal patella (PAT).

BOVINE CARTILAGE SAMPLES

For study II and III, intact bovine patellofemoral joints (n = 8), were obtained from the local slaughterhouse (Atria Oyj, Kuopio, Finland). Cartilage plugs without subchondral bone (dia. = 4.0 mm, n = 24 from patella (PAT, n = 8 (study II); n = 4 (study III)), lateral patellar groove (LPG, n = 4, medial tibial plateau (TMP, n = 4) and femoral medial condyle (FMC, n = 4) were immersed in phosphate buffered saline (PBS, Euroclone, Pero, Italy) and frozen immediately at $-20\,^{\circ}\mathrm{C}$. Prior to experiments, all samples were thawed for a minimum for one hour in PBS.

5.1.2 Mechanical measurements

A custom–made mechanical tester with a high resolution (0.1 μm) actuator (PM500–1A; Newport, Irvine, CA), a force transducer (0.005 N resolution) (Sensotec, Columbus, OH), and custom–made software for measurement control and data acquisition (Lab–View; National Instruments, Austin, TX) was used for the biomechanical measurements (figure 5.2).

Young's modulus was determined with a stepwise stress–relaxation technique (four steps, 5% strain up to a maximum strain of 20%) [96]. Dynamic modulus test was conducted using 1 Hz sinusoidal loading and a 1% strain amplitude [135].

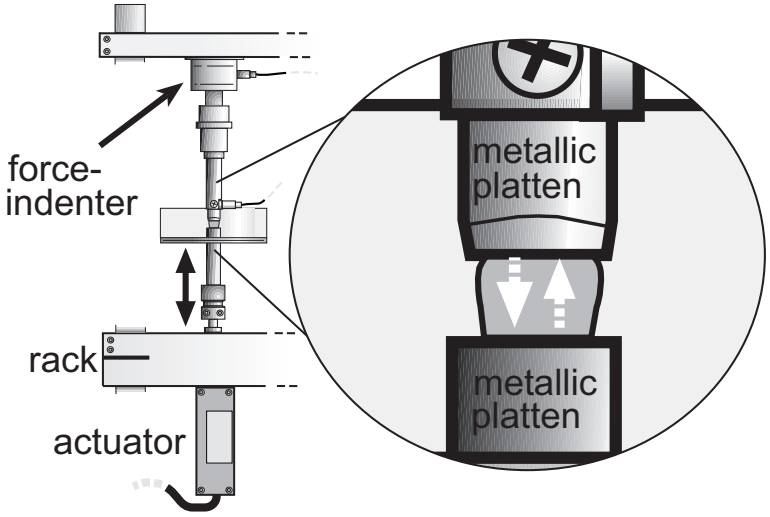

Figure 5.2: Setup for mechanical testing of articular cartilage. To minimize the friction and to permit as free motion as possible between the sample and the metallic plates, synovial fluid was used to lubricate the interfaces.

5.1.3 MRI measurements

In studies I, II and III, articular cartilage samples were imaged with a 9.4 T Oxford 400 NMR vertical magnet and an SMIS console (SMIS Ltd., Surrey, UK) equipped with a 5–mm high–resolution transmitting/receiving spectroscopic volume coil (Varian Associates Inc., Palo Alto, CA) at $25\,^{\circ}\mathrm{C}$.

In T_2 measurements, the articular surface was oriented perpendicular to the static field in order to take advantage of the dipolar coupling in revealing the collagen arrangement with tissue depth. T_2 relaxation mapping was performed with a single echo spin echo sequence (TR = 2500 ms, six TEs between 14 and 84 ms) with minimized sensitivity to diffusion [53].

In studies I and III, T_1 relaxation time mapping was conducted with a saturation recovery sequence (TE = 14 ms, six TRs between 200–5000 ms). For studies I and II, the T_1 imaging was repeated for dGEMRIC ex-

periments after 2.5 hr equilibration in 1mM Gd-DTPA^{2-} (TR = 100–1500 ms).

For study II, $T_{2\mathrm{Gd}}$ imaging was performed (*i.e.* T_2 mapping in the presence of Gd-DTPA^{2-}). Depthwise $T_{1\mathrm{Gd}}$, T_2 and $T_{2\mathrm{Gd}}$ profiles were calculated by averaging three pixels along the articular surface. $T_{1\mathrm{Gd}}$ and $T_{2\mathrm{Gd}}$ were defined as described earlier (equation 3.19). The in–plane resolution was 39 μm across cartilage thickness with 1–mm slice thickness, with six signal averages, 10–mm FOV with 256 x 64 imaging matrix, TR = 1500 ms. The sequences used are presented in figure 5.3.

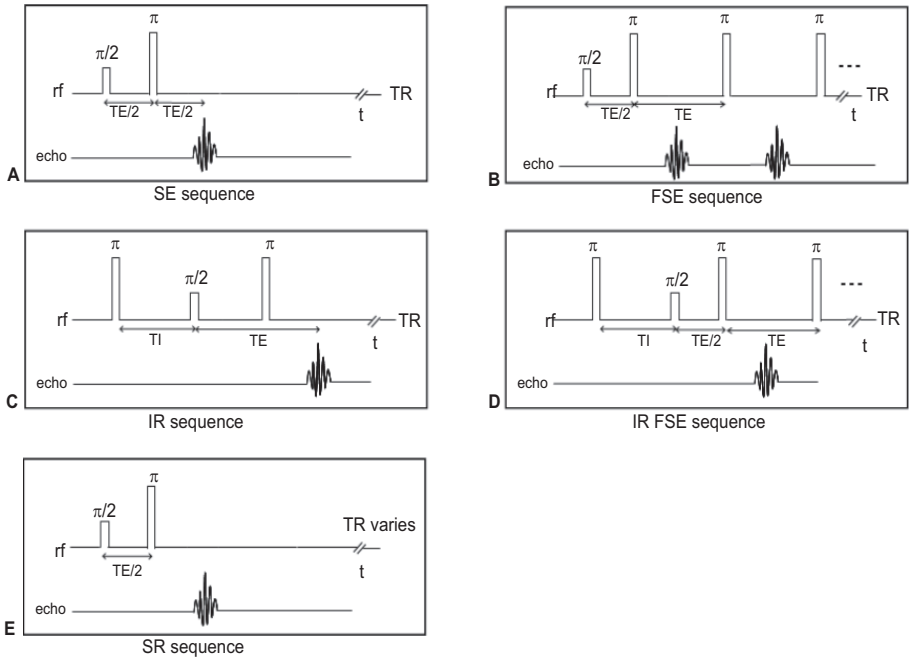

Figure 5.3: (A) Spin echo sequence, (B) fast spin echo sequence, (C) inversion recovery sequence, (D) inversion recovery fast spin echo sequence and (E) saturation recovery sequence used in the present studies.

5.1.4 Polarized light microscopy

The quantitative collagen fibril arrangement in cartilage was evaluated by PLM by analyzing the optical birefringence (BF) [5, 17]. Collagen has the capacity to rotate the plane of polarized light, *i.e.*

$$BF = \frac{\alpha\lambda}{\pi l} = \frac{\lambda}{\pi l}\arcsin\sqrt{\frac{I - a_F}{b_F I_0}}, \tag{5.1}$$

where α is the rotation angle of the polarized plane, λ is the wavelength of monochromatic light, l is the optical path length, I is the intensity of emerging light, I_0 the intensity of light after the first polarizer, and a_F and b_F are optical constants.

Cartilage plugs were cut into two halves in a vertically randomized direction, fixed in formalin, decalcified, and embedded in paraffin. Later, the samples were cut into 5–μm sections. The sections were placed in between the perpendicularly crossed polarizers under monochromatic light, with a $\lambda/4$ compensator in between the polarizers. The light transmitted through the system is dependent on the collagen fiber orientation, giving rise to an image. Polarized light microscopy (PLM) measurements were performed using a Leitz Ortholux BK–2 polarized light microscope (Leitz, Wetzlar, Germany), 6.3x magnifying strain–free objective, a cooled 12–bit CCD camera (SenSys, Photometrics, Tucson, AZ, USA), a monochromatic light source (λ = 594 $\pm$ 3 nm) and a pair of motor–controlled crossed polarizers. Spatial resolution achieved was 8.9 μm.

Low BF refers to a tissue structure with a low degree of collagen fiber organization. This can typically been seen in the middle zone. High BF values reflecting the presence of organized collagen fibers are usually detected in the superficial and deep zones (figure 5.4).

BF images were converted from grayscale microscopic images recorded from the cartilage surface to subchondral bone [5, 17]. Six independent sections were imaged and averaged from each sample to minimize the effect of sample–dependent variations. BF profiles were further inverted and compared with the T_2 profiles. Degeneration and maturity of the samples [137] and static compression methods have been shown to affect on the angle of collagen fibers detected by the PLM method and the number of zones in articular cartilage [3].

5.1.5 Measurement of PG content

In study III, small pieces were cut from the edges of the MRI samples for Safranin–O–staining. These were embedded in paraffin and cut into 3–μm sections [145]. Optical density (OD) microscopy of Safranin O–stainings was performed to determine the PG content in the tissue. Safranin–O, a cationic dye, attaches itself to GAGs, and the OD is linearly related to the amount of fixed charges [92, 93]. The linear absorbance A_l of a microscopic section can be calculated from

$$A_l = -log(T_l), \tag{5.2}$$

where transmittance $T_l = I/I_0$ is the ratio of the transmitted and initial intensity of light. Linearity of A_l and a correct filter set makes it possible

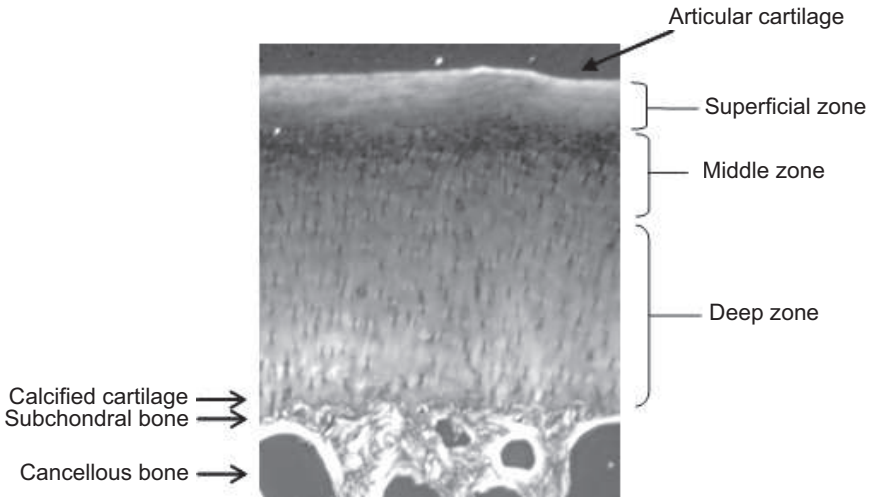

Figure 5.4: Histological zones presented in PLM-image.

to relate the transmission of light to a specific OD value, reflecting the concentration of PGs in the microscopic sections [92, 93].

OD measurements were conducted using the same equipment as used for PLM imaging without polarizers. Monochromatic light source (λ = 492 $\pm$ 5 nm) and neutral density filters were used with a 4.0x magnifying strain–free objective, yielding a spatial resolution of 6.9 μm. Five independent sections were analyzed and averaged (figure 5.5). The OD (absorbance) was calculated using the calibration curve [93, 145].

5.1.6 Measurement of water content

In study III, pieces of tissue adjacent to the MRI samples were used for bulk water content analysis. The samples were soaked in PBS (4 hours on average) and weighed using a sensitive high–resolution balance (Mettler AE240, Mettler–Toledo AG, Switzerland). This was repeated three times with all the results being averaged. Dry weight measurements were conducted after 72 hours of freeze–drying. The water content was determined as 100% subtracted by the ratio of dry and wet weight.

5.2 *In vivo* experiments

5.2.1 ACT patients

For study IV, patients (n = 12, age 37 $\pm$ 8 years) with symptomatic local cartilage defects in the femoral condyle and/or trochlea underwent ACT

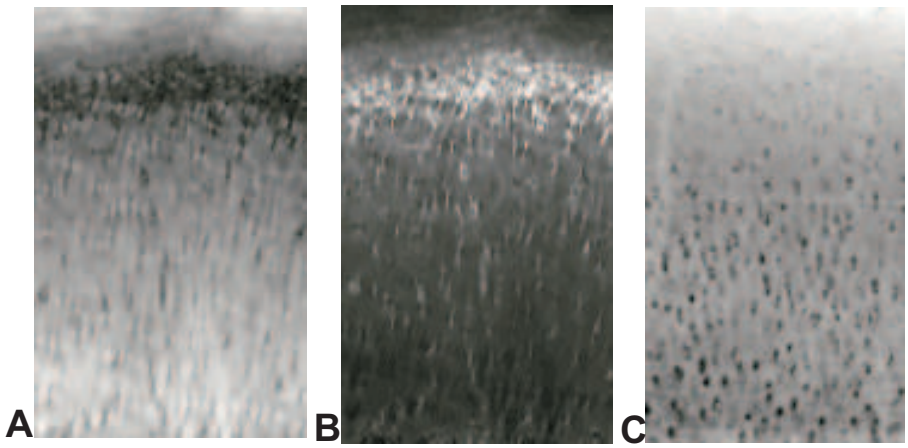

Figure 5.5: Grayscale polarized microscopic (A) BF, (B) $1/BF$ image and (C) optical density (OD) image of Safranin O–stained PGs.

surgery. The study group consisted of patients with 13 lesions in FMC (n = 6), FLC (n = 3) and trochlea (n = 4). An osteochondritis dissecans (OCD) lesion was detected in four patients. Each patient underwent a two–step ACT procedure: an initial arthroscopic evaluation and a cartilage biopsy of a less–weight bearing healthy articular cartilage area [24]. Chondrocytes were isolated from the cartilage biopsy and the number of the chondrocytes was increased in a cell culture in laboratory conditions. After a few weeks, the chondrocytes were implanted via an injection underneath an autologous periosteal flap sutured over the debrided cartilage lesion [24, 119] (figure 5.6).

5.2.2 MRI measurements

The patients were examined at 10 to 15 months after the surgery by MRI at 1.5 T (GE Signa 1.5 T, Milwaukee, WI) using a quadrature transmit and receive imaging extremity coil. First a clinical MRI exam of the knee joint was conducted, including a PD–weighted fast spin echo (FSE) series with fat suppression in coronal (TR = 3140 ms, effective TE = 25 ms, echo train length (ETL) of 9, 256x224 imaging matrix, 0.63x0.71 mm in–plane resolution), sagittal (TR = 3500 ms, effective TE = 41 ms, ETL = 8, 256x256 matrix, 0.63x0.63 mm in–plane resolution) and axial directions (TR = 2800 ms, effective TE = 25 ms, ETL = 8, 256x224 matrix, 0.63x0.71 mm in–plane resolution), coronal PD–weighted FSE series without fat suppression (TR =

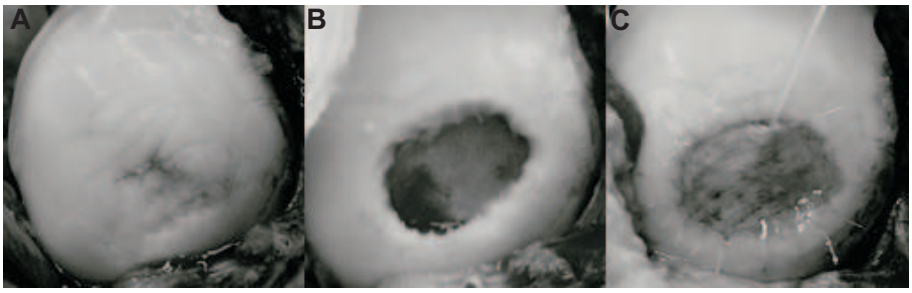

Figure 5.6: Autologous chondrocyte transplantation. (A) Degenerated articular cartilage was removed (B), autologous periosteal flap was sutured over the debrided cartilage lesion and (C) chondrocytes were injected under it.

2500 ms, effective TE = 21 ms, ETL = 6, 256x256 matrix, 0.63x0.63 mm in–plane resolution). The field–of–view in PD–weighted images was 16–cm. A sagittal T_1–weighted spin echo series was conducted with TR = 600 ms, effective TE = 9 ms, 512x320 matrix, 32–cm FOV, 0.63x1.00 mm in–plane resolution. In every imaging series, the slice thickness was 3–mm.

After the clinical knee examination T_2 relaxation time mapping was performed. A series of sagittal and coronal single–slice FSE measurements from the center of the graft were conducted with varying echo times (TR = 2000 ms, six effective TEs between 18 and 110 ms, ETL = 9, 512x512 matrix, 16–cm FOV, 0.31x0.31 mm in–plane resolution, 3–mm slice).

Following the T_2, an intravenous injection of 0.2 mM/kg Gd-DTPA^{2-} (Schering AG, Berlin, Germany) was given to permit the dGEMRIC experiments. After a 2–h delay, the T_1 relaxation time was determined at the location of the T_2 measurement, using a series of single slice inversion recovery FSE measurements in the sagittal and coronal planes (TR = 1800 ms, ETL = 9, TE = 17 ms, seven TIs between 50 and 1650 ms, 512x512 matrix, 16–cm FOV, 0.31x0.31 mm in–plane resolution, 3-mm slice). Coronal T_2 and dGEMRIC data were available for nine grafts. The sequences in use are presented in figure 5.3.

5.3 Data analysis

In study I, the non-parametric Friedman test and the Friedman post hoc test for several dependent samples were utilized in order to assess the topographical variations in MRI and biomechanical parameters (SPSS Software; SPSS Inc., Chicago, IL). The Pearson's linear correlation test was used to analyze the interrelationships between the MRI and biomechanical parameters. Bulk values of each parameter were calculated as the mean value of the profiles, whereas the surface values for MRI experiments consisted of the averages calculated from the 3x3 pixels on the cartilage surface.

Study II concentrated on the comparison of PLM– and T_2–profiles (figure 6.4). The profiles were equalized by downsampling the BF data to match the MRI resolution. A truncation from deep cartilage was performed to equalize the profile vector lengths [134]. A pixel–by–pixel analyzed linear Pearson correlation was performed between the resampled $1/BF$ profiles and surface-matched depthwise (from cartilage surface to subchondral bone) T_2 and $T_{2\mathrm{Gd}}$ datasets for each sample, and for pooled data (SPSS software, SPSS inc., Chicago, IL). The Wilcoxon signed ranks test was used to compare the difference between T_2 and $T_{2\mathrm{Gd}}$.

From $1/BF$ and T_2, the profiles thickness of histological zones were determined and compared. The zone–boundaries were determined for each rising/declining edge as the half–maximum value, a method adapted from Xia *et al.*, 2001 [198]. A custom-made MATLAB program (MathWorks Inc. , Natick, MA, USA) was used for the calculations. The Bland–Altman plot was used to assess the agreement of MRI and PLM techniques for the determination of the locations of the lamina boundaries [18]. The Kruskal–Wallis post hoc test was applied in order to investigate the significance of differences in zone thicknesses. To analyse the reproducibility of the measurements, the coefficient of variation (CV%) for depthwise and deep tissue data was calculated [58].

In study III, the depthwise MR and OD data were compared. In order to enable a sample–by–sample comparison, the profiles were linearly interpolated to 10 μm spatial resolution and truncated from the deep tissue to the shortest length. Bulk values of each parameter were calculated as the mean value of these profiles. Using the bulk values of the parameters and bulk water content, statistical comparisons between the different sites in the knee joint were conducted, applying Friedman post hoc test. Pearson's linear correlation and the first order partial correlation test were used to demonstrate the associations between the parameters.

In study IV, T_2 relaxation time maps were calculated by means of a

mono–exponential two–parameter fitting in MATLAB (version 7.0.4, Mathworks Inc., Natick, MA) using all time points. T_1 relaxation time maps were calculated using a three–parameter fitting. Sagittal and coronal values were determined from the manually segmented full thickness ROIs, matched in location and size (area 6–9 mm^2, mean 7$\pm$1 mm^2) from the central portion of the graft. Superficial and deep half of the tissue in each graft were also studied. Relaxation time values were similarily determined for control tissue, *i.e.* in the sagittal plane, the cartilage adjacent to the graft, with normal signal intensity, was chosen. In the proton density–weighted images, the grafts in the posterior part of the joint had anterior control ROIs, and the grafts positioned at the anterior part had a control ROI at the posterior part. In the coronal orientation, control ROIs were chosen from the respective site of the contralateral side of the joint. PD–weighted images were categorized based on the signal intensity as hypo–, iso– or hyperintense, as compared to the surrounding cartilage. Relaxation time values were compared with the non–parametric Wilcoxon's signed ranks test (SPSS Inc., Chicago, IL, USA). The Pearson correlation coefficient was determined for T_2 and dGEMRIC values for control and graft tissue. A Kruskal–Wallis test was used to determine the dependence between the PD–weighted signal intensity and the quantitative MRI parameters of the grafts. Relaxation time values of grafts at different anatomical locations (*i.e.* femur and trochlea) were compared using the Mann–Whitney test.

CHAPTER VI

Results

6.1 Topographical variation of cartilage properties

In study I, topographical biomechanical and MRI parameters were investigated to characterize the structural and functional properties of human articular cartilage. Statistically significant site-dependent differences ($p < 0.05$, Friedman post hoc test) were revealed in both the mechanical properties and the relaxation parameters of cartilage (figure 6.1). Statistically significant correlations (r = 0.24 – 0.87) were observed between the MRI and mechanical parameters in the human knee cartilage (figure 6.1). The highest value for Young's modulus was recorded at FMC (1.16 $\pm$ 0.36 MPa) and for the dynamic modulus at FLC (10.04 $\pm$ 3.69 MPa), whereas the lowest values were found at PAT (E_{eq} = 0.56 $\pm$ 0.24 MPa, G_d = 4.47 $\pm$ 2.22 MPa). With respect to the MRI parameters, the longest T_1 relaxation time occurred at TLP (1830 $\pm$ 150 ms), T_2 relaxation time at TMP (37 $\pm$ 7 ms) and $T_{1\mathrm{Gd}}$ time at FLC (640 $\pm$ 190 ms). PAT cartilage exhibited the shortest T_1 (1590 $\pm$ 330 ms) and $T_{1\mathrm{Gd}}$ (470 $\pm$ 60 ms) relaxation times and the FG cartilage displayed the shortest T_2 relaxation times (30 $\pm$ 4 ms). The highest and lowest gadolinium concentrations were detected at PAT (0.41 $\pm$ 0.07 mM) and at FMC (0.30 $\pm$ 0.10 mM), respectively (figure 6.2).

In study III, significant variations ($p < 0.01$, Friedman post hoc test) were revealed for the T_1 bulk and OD values between the sample groups TMP–LPG, for the T_2 bulk and water content between the groups TMP–PAT (figure 6.3).

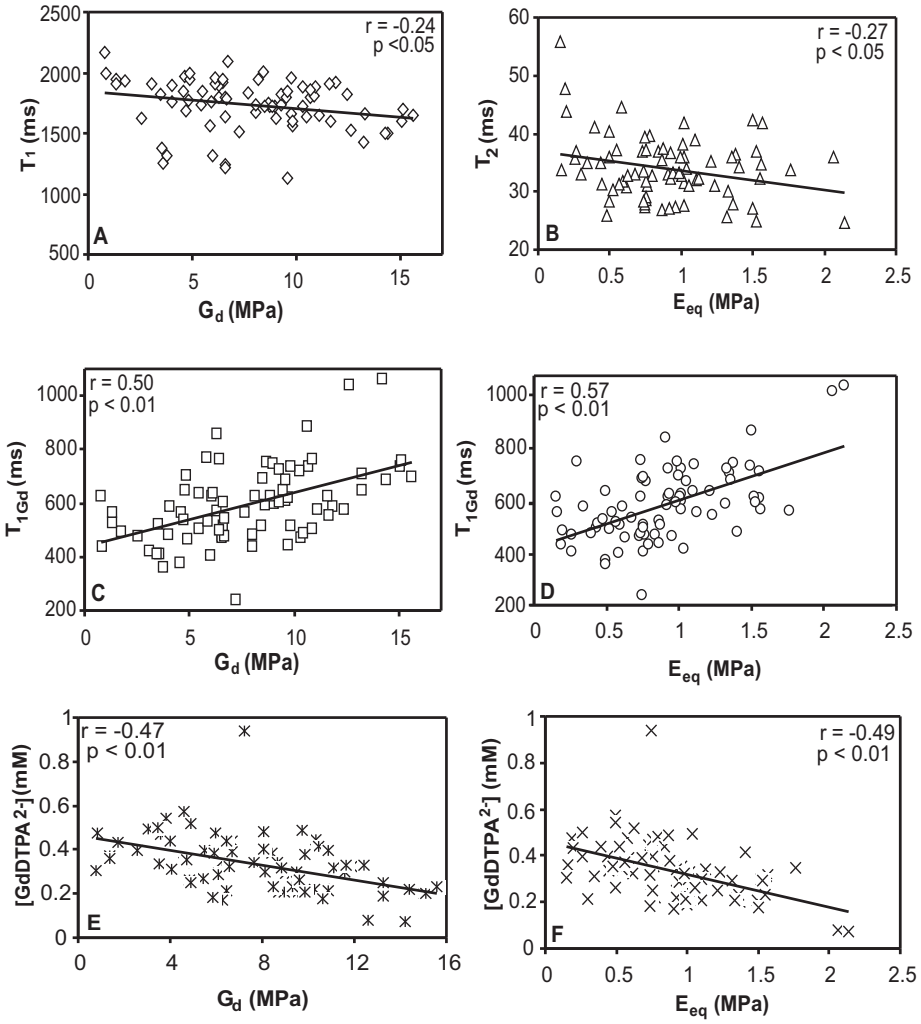

Figure 6.1: Statistically significant correlations (linear Pearson correlation) between the biomechanical and bulk MRI parameters.

6.2 T_2 in the presence of Gd-DTPA^{2-}

Average T_2 and $T_{2\mathrm{Gd}}$ bulk relaxation times were 34.2 $\pm$ 5 ms and 33.7 $\pm$ 5 ms, respectively. Wilcoxon signed ranks test revealed no significant differences between bulk T_2 and $T_{2\mathrm{Gd}}$ ($p < 0.26$). Bulk $T_{2\mathrm{Gd}}$ relaxation time values correlated with T_2 values (r = 0.73, $p < 0.05$, n = 65).

Spatial T_2 and $T_{2\mathrm{Gd}}$ maps were compared against PLM analysis. The mean thicknesses of superficial (i), intermediate (ii) and deep (iii) zones,

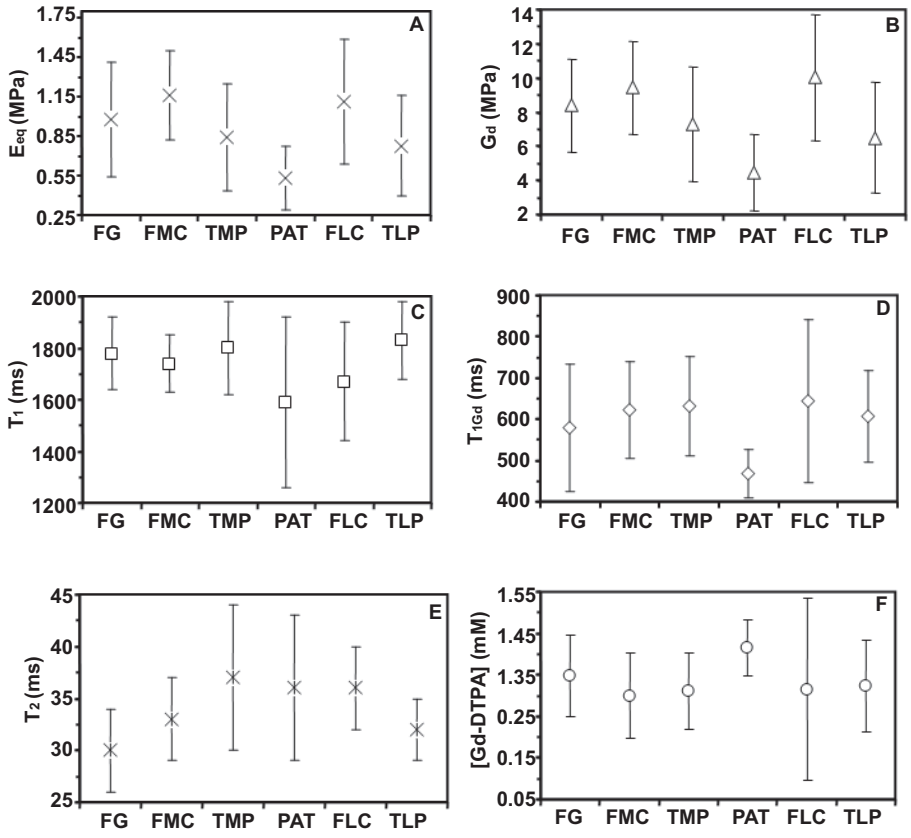

Figure 6.2: Site-dependent variations in the biomechanical and MRI parameters. Values are presented mean ± SD.

as determined from T_2, $T_{2\mathrm{Gd}}$ and PLM profiles for all samples, were similar (table 6.1). Zone thicknesses defined from T_2 and $T_{2\mathrm{Gd}}$ profiles correlated significantly ($p < 0.01$) between the zones i (r = 0.55), ii (r = 0.74) and iii (r = 0.95), respectively (table 6.2). T_2 and $T_{2\mathrm{Gd}}$ relaxation time maps of intact human articular cartilage revealed the classical tri–laminar structure (figure 6.4).

6.3 Native T_1 in cartilage

In study II, the ability of MRI parameters to reflect water content was assessed. The water content showed a strong negative correlation (r = – 0.81 and r = – 0.60, $p < 0.01$) with R_1 and R_2 (figure 6.5). T_1 and T_2 relaxation rates were statistically interrelated (r = 0.52, $p < 0.05$). After adjustment

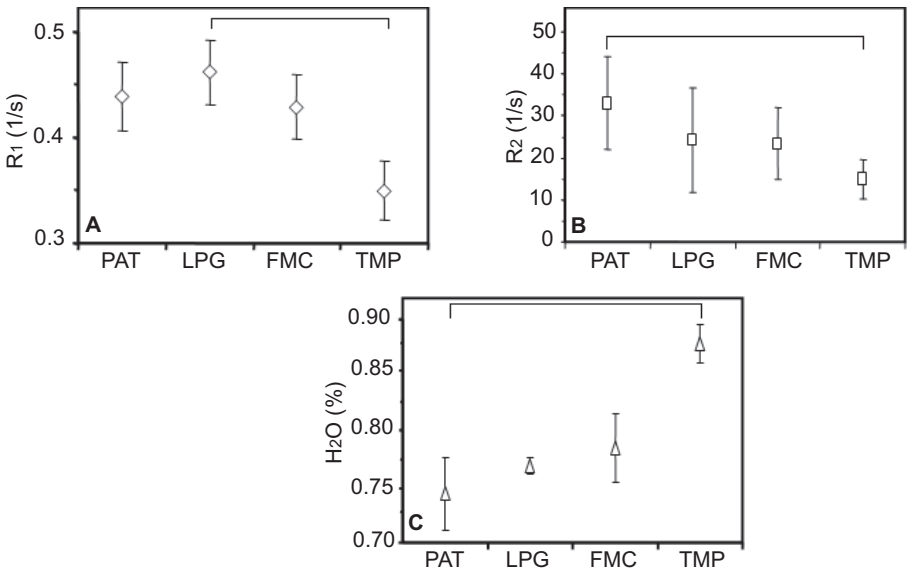

Figure 6.3: Topographical variations in the R_1 and R_2 relaxation times and water content of the bovine knee articular cartilage (mean $\pm$ SD).

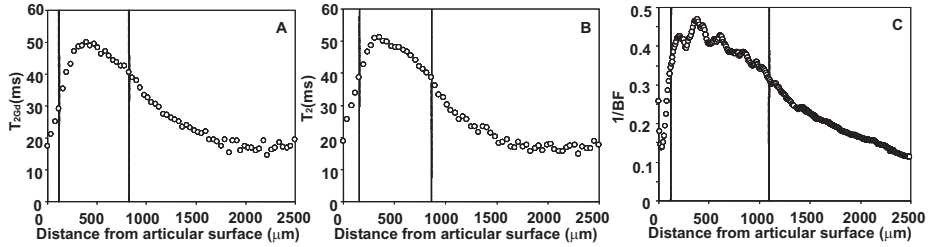

Figure 6.4: The zone–boundaries determined for each rising/declining edge as the half maximum value, a method adapted from Xia *et al.*, 2001. Zone–boundaries marked with dash line in (A) $T_{2\mathrm{Gd}}$, (B) T_2 and (C) $1/BF$ profiles.

for OD, the first order partial correlation showed significant associations between water content and R_1 ($r =$ –0.48, $p < 0.05$) or R_2 ($r =$ –0.50, $p <$ 0.05). After adjustment for water content, R_1 or R_2 did not show a significant association with OD.

Table 6.1: Mean values for zone thickness (i–iii) as detected with PLM or MRI (n = 65).

	T_2[1] (mm)	$T_{2\mathrm{Gd}}$[2] (mm)	1/BF[3] (mm)
i	0.14 ± 0.06*	0.15 ± 0.07*	0.21 ± 0.15*
ii	0.58 ± 0.22	0.61 ± 0.23	0.59 ± 0.24
iii	1.14 ± 0.50	1.10 ± 0.50	1.03 ± 0.50

*statistically significant differences (p<0.01) detected with Kruskall–Wallis post hoc test between groups 1–3 and 2–3 for zone i. For zones ii and iii, no significant differences were detected.

Table 6.2: Correlation coefficients for zone thickness between the different imaging techniques.

	Zone i	Zone ii	Zone iii
T_2 vs $T_{2\mathrm{Gd}}$	0.55**	0.74**	0.95**
T_2 vs $1/BF$	0.24	0.52**	0.89**
$T_{2\mathrm{Gd}}$ vs $1/BF$	0.27*	0.45**	0.89**

*statistically significant differences, *p<0.05, **p<0.01, Pearson linear correlation.

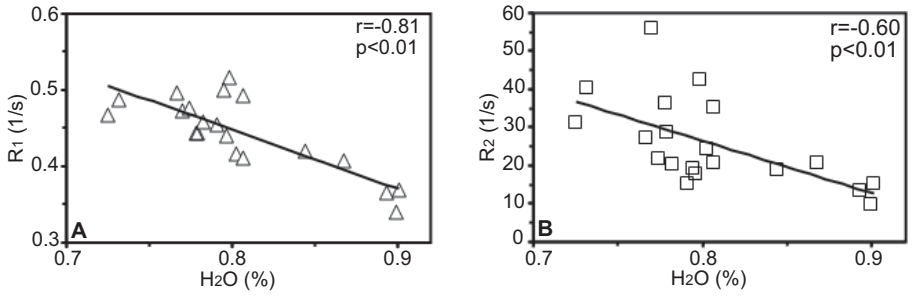

Figure 6.5: Pearson linear correlations between water content and (A) R_1 or (B) R_2 on bovine articular cartilage.

6.4 Evaluation of cartilage repair

In study IV, the qMRI technique was evaluated to assess cartilage repair. All 13 ACT grafts had been filled by the repair sites equal to or above the level of adjacent native tissue. The matrix appeared homogenous and

lacked the laminar structure of control cartilage. There were also no discernible fissures between the repair and adjacent normal tissue (figure 6.6).

Bulk, superficial and deep graft tissue had significantly longer T_2 relaxation times in the sagittal plane, as compared to control tissue ($p < 0.001$, $p = 0.019$ and $p = 0.004$) (table 6.3). In the coronal plane, ACT grafts showed significantly longer T_2 values for bulk tissue as well as for the deep tissue ($p = 0.051$ and $p = 0.038$) (table 6.4). The superficial tissue revealed no significant differences in T_2 values. dGEMRIC values did not exhibit any significant differences in sagittal and coronal directions between graft or control tissue.

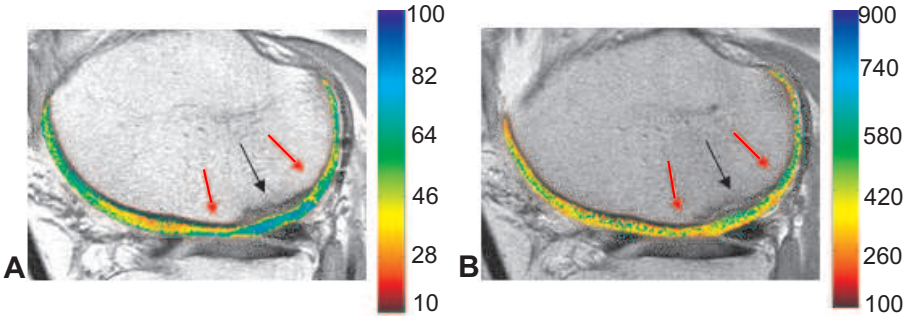

Figure 6.6: (A) T_2 map and (B) dGEMRIC ($T_{1\mathrm{Gd}}$) map of an ACT patient. Control tissue is marked with a red arrow, the graft with a black arrow. In this particular patient, the graft shows a higher dGEMRIC value and the T_2 map shows higher T_2 values for graft when compared to control tissue.

Table 6.3: T_2 and dGEMRIC times of knee cartilage in the sagittal plane for ACT patients (n = 13).

	T_2		dGEMRIC	
	graft	control	graft	control
bulk	61 ± 8*	46 ± 5	437 ± 87	422 ± 55
surf	61 ± 9*	51 ± 11	413 ± 86	411 ± 57
deep	59 ± 10*	40 ± 7	458 ± 101	432 ± 78

*statistically significant differences in T_2 values detected with Wilcoxon signed ranks test between graft and control tissue in bulk (P=0.001), superficial (P=0.019) or deep (P=0.004) tissue. For dGEMRIC values, no significant differences were detected.

Table 6.4: T_2 and dGEMRIC times of knee cartilage in the coronal plane for ACT patients (n = 13).

	T_2		dGEMRIC	
	graft	control	graft	control
bulk	58 ± 8*	52 ± 10	432 ± 97	440 ± 72
surf	60 ± 8	55 ± 10	438 ± 98	438 ± 48
deep	60 ± 11*	48 ± 13	428 ± 121	444 ± 107

*statistically significant differences in T_2 values detected with Wilcoxon signed ranks test between graft and control tissue in bulk (P=0.051) or deep (P=0.038) tissue. For dGEMRIC values, no significant differences were detected.

CHAPTER VII

Discussion

7.1 MRI and structural/functional properties of native cartilage

dGEMRIC, T_1 and T_2 relaxation times revealed statistically significant topographical variations among different sites of the human and bovine joint. Although these differences were not always fully matched with the alterations in mechanical properties, the present data does indicate that quantitative MRI parameters are significantly associated with the mechanical properties of articular cartilage (I). The finding is in good agreement with the previous literature [9, 99, 135, 138, 159]. Considering the significant linear correlations between the MRI and mechanical parameters, the *in vitro* findings of MRI underline the potential of MRI as a biomarker for cartilage biomechanics.

dGEMRIC has proven to be a useful technique for estimating the PG concentration of articular cartilage, both *in vitro* and *in vivo*. However, at its best, MRI predicted less than 50% of the variations in compressive stiffness for pooled cartilage samples (I). This may in part be attributable to the heterogeneous sample material (varying age of patients) and the topographical differences in cartilage properties, but it also reflects the fact that the mechanical properties of cartilage in unconfined compression are not solely determined by the PGs but are also strongly affected by the content and organization of tissue collagen [95]. In addition, the limitations of dGEMRIC technique, *i.e.* the relaxivity value that is assumed to be constant through tissue depth and time of equilibration reached, may affect the correlation between the MRI and compressive stiffness. Further, certain joint areas may possess more uniform structural features than others, this possibly being controlled by the degree of local weight–bearing in the

area. Samosky *et al.* described a higher load response and dGEMRIC values in the submeniscal region than in the central region of the samples [159]. Also the correlations between $T_{1\mathrm{Gd}}$ and the load response in the submeniscal area were higher than in the central areas of the samples.

This present study and previous work [138] suggests that simple bulk T_2 values do not adequately characterize the functional properties of the tissue, and hence more advanced analysis schemes for T_2 are required. In *in vitro* and *in vivo* imaging geometry, such differences in T_2 values may be caused in part by the varying orientation of the articular surface in the B_0 field due to the magic angle effect [127].

The depth–wise variation of both T_2 and $T_{2\mathrm{Gd}}$ were highly correlated with the collagen network architecture, as evaluated with PLM for normal articular cartilage (II). Zonal thickness values determined from MRI and PLM profiles agreed with each other. Although the contrast agent slightly modified the T_2–profile, as revealed by comparison of T_2 and $T_{2\mathrm{Gd}}$–data, it had a minor impact on the structural information analyzed from the $T_{2\mathrm{Gd}}$ profiles. As dGEMRIC serves as a noninvasive MRI technique to estimate cartilage proteoglycan content [14], it would be advantageous to merge both techniques into one imaging session. Earlier, Nieminen *et al.* proposed the use of a back–calculating method *in vitro* [132]. Van Breuseghem *et al.* applied this method *in vivo*, introducing a method to combine the imaging sessions which both simplified and made faster the clinical applicability [183].

When Gd-DTPA^{2-} is present, T_2 is reduced more in the superficial than in deeper part of the tissue, creating a nonuniform weighting on T_2 maps of full thickness cartilage. This was verified in the present study. Further, the weakest correlation between T_2 and $T_{2\mathrm{Gd}}$ was established in the superficial lamina, the most thin and most prone lamina for positioning errors and partial volume effects. This assumption is supported by the finding that reproducibility of the T_2 measurements was weakest in the superficial lamina. While the current study involved intact cartilage, in pathological tissue the contrast agent concentration can reach elevated levels that may cause a significant shortening of T_2 [118].

In the present study, native T_2 relaxation times were generally short and occasionally the measurements resulted in a nonphysical result *i.e.* $T_{2\mathrm{Gd}}$ was higher than T_2. Given the bell–shaped form of T_2 profiles, it is likely that an apparent increase in T_2 can inherently occur somewhere along the profiles, provided that the T_2 maxima of the two profiles are non–perfectly matched. Moreover, storage and handling of the samples may have an impact on the variations in T_2 and $T_{2\mathrm{Gd}}$ results [51].

Back–calculation for correcting $T_{2\mathrm{Gd}}$ was also performed, without this having any positive impact on the results. The constant relaxivity value throughout the tissue depth also raises the possibility for an error. However, the possible spatial mismatching of the MRI and PLM profiles is likely to present a more significant error factor. For degenerated, PG–depleted tissue with a pathologically high gadolinium concentration, back–calculation may be necessary or, alternatively, lower bath concentrations should be used [132].

Other possible error factors need also to be considered. In the microscopic studies, PLM analyses were conducted on the tissue adjacent to the MRI samples. This might also affect the results. Second, microscopic sections were prepared from osteochondral blocks whereas samples for MRI were detached from the underlying bone. This may give rise to inconstant swelling leading to imprecise profiling and zone matching. Third, PLM profiles consist of an average of six sections, resulting in tissue that might not be represented in T_2 or $T_{2\mathrm{Gd}}$ profiles. Fourth, sample processing for PLM may involve cartilage shrinkage [79], which would impair the spatial matching of zones. Despite the limitations, the present results indicate that T_2 and Gd-DTPA^{2-} enhanced imaging sessions can be combined, when focusing on the properties of intact cartilage.

Formerly, T_1 has been considered as non–specific for any cartilage macromolecules and it does not exhibit anisotropy in articular cartilage [77]. No association was found between the R_1 and PG content measured with OD, supporting the conclusion that native T_1 seems to be free from structural effects and, furthermore exhibits a primary correlation with water content in articular cartilage (III). Further, a monotonic increase of T_1 relaxation time with water content of gelatin and cotton phantoms [83] and various tissues from mice (fat, liver, spleen, kidney, tumor, fetus) [84] has been reported. T_1 has been shown to depend on the water content and is less independent of tissue type [84].

One limitation of the present study is the analysis of bulk values, because the cartilage water content depends significantly on the tissue depth [25, 153, 162]. Also, T_1 depends strongly on the field strength, and the suitability of R_1 as a water measure in lower field strengths needs to be studied. Further, a relatively small number of samples were analysed (n = 20), which may have had an impact on the correlation analyses. Finally, the relationship between relaxation rates and collagen content was not studied.

In the present study (III), T_2 relaxation rate correlated with the cartilage water content, which is in line with the previous studies where T_2–weighted imaging has been studied as a biomarker for cartilage water con-

tent [106, 109, 162]. However, the T_2 relaxation time is dependent also on the orientation of the collagen network through interactions between water bound and collagen fibrils, *i.e.* the magic angle effect [60, 136, 198]. The shape of a typical T_2 relaxation profile is not in agreement with the known depth–wise changes in water content, whereas the monotonically decreasing depth–wise T_1 resembles the characteristic water content profile [153]. Since native T_1 relaxation time measurements may be required for a reliable dGEMRIC experiment [188], the assessment of native T_1 alone can provide further aspect into such experiment as a surrogate marker for the water content.

Significant associations were observed between the various MR and compositional parameters, pointing to complex interactions between different constituents. Native T_1 relaxation time properties have also been shown not to correlate with the PG content [14]. The former findings between T_1 and mechanical properties [99, 135, 189] are likely explained by the observed dependence of T_1 on the cartilage water content.

7.2 MRI and cartilage repair

In the present study, the dGEMRIC values for repair and control tissue were similar. The results suggest that PGs are replenished to the level of adjacent native cartilage within one year. Previous studies have shown that ACT repair tissue can reach dGEMRIC values comparable to normal cartilage, evidence of proteoglycan replenishment [55, 184]. Occasionally, ACT grafts had a higher dGEMRIC index than control tissue, suggesting PG replenishment above the normal levels, or perhaps that the repair tissue differs from that of normal cartilage and consequently bias the dGEMRIC results. It is possible that these results are affected by the constant relaxivity value and/or native T_1 results reflecting the water content in the repair tissue.

T_2 relaxation time values were significantly higher for repair tissue than for native tissue. T_2 relaxation time of cartilage is typically short due to the effective dipolar interaction of collagen–associated water, and changes as a function of the collagen fibril arrangement in the static magnetic field [197]. Higher T_2 values in ACT repair tissue and the lack of the typical laminar appearance suggests that the collagen network lacks the classical three–dimensional structure of normal adult articular cartilage. A recent study using an animal model for spontaneous cartilage repair showed significantly shorter T_2 relaxation times for fibrous repair tissue as compared to control tissue [132]. Quantitative T_2 mapping can also reveal differences in repair tissues formed after different surgical cartilage

repair procedures [191]. Trattnig *et al.* showed, that 19–24 months after the matrix-associated autologous cartilage transplantation (MACT) repair, tissue T_2 profiles normalized over time toward the control sites [177]. This is different to the present findings and gives rise to speculation that the repaired tissue produced by different surgical procedures may vary and different tissue types may be distinguished using T_2 mapping. The present results emphasize how dGEMRIC and T_2 can provide complimentary information on engineered cartilage and a more comprehensive characterization is possible by combining these two techniques.

The curvature of the joint surfaces and thereby the magic angle effect represent a possible source of error in the T_2 measurements when comparing sagittal T_2 values of the graft to the adjacent cartilage. Also the adjacent cartilage may have been affected during or after the implantation. To eliminate these possible effects, measurements in the coronal direction were also conducted to clarify these issues. This preliminary study was also limited by the number of patients examined.

The variations of the T_2 or dGEMRIC results in the sagittal and coronal directions point to errors in the slice positioning and/or compositional and structural variation in different parts of the grafts. Also, a multi–echo sequence might have produced a more accurate estimate of cartilage T_2 relaxation time than the fast spin–echo approach [111, 117]. Finally, histological control data is not available to verify the qMRI findings.

In summary, a combination of T_2 and dGEMRIC techniques can provide a more complete characterization of the repair tissue produced by ACT. If T_1 and T_2 measurements could be conducted simultaneously during the same imaging session in the presence of the contrast agent, this would further simplify the combination of the techniques and improve their clinical applicability.

CHAPTER VIII

Conclusions

In the present study, qMRI methods have been used to characterize the structural and mechanical properties of native and repaired articular cartilage and validated against established reference methods, *i.e.* mechanical testing and histological methods. The following conclusions can be drawn:

1. MRI parameters (T_1, T_2, and particularly dGEMRIC) in human knee articular cartilage *in vitro* moderately reproduce the topographical differences in compressive moduli, and display significant linear correlations with the mechanical parameters. Thus, MRI may serve as a biomarker for cartilage biomechanics. MRI parameters can also reveal additional site–dependent differences that are not observed in evaluations of compressive properties.

2. Combining dGEMRIC and T_2 analyses, in the presence of Gd-DTPA^{2-}, it is possible to obtain PG and collagen related information on cartilage in a single MR imaging session. Gd-DTPA^{2-} has a minor effect on T_2 relaxation time. However, the spatial variation of T_2 and the zonal information extracted from intact cartilage is highly comparable to the findings from native T_2 and PLM.

3. T_1 relaxation rate showed a significant linear relationship with the water content in cartilage, but was not associated with matrix PGs. The results suggest that R_1 could be used as an independent means of evaluating the water content in articular cartilage.

4. According to T_2 measurements, ACT repair tissue at 10–15 months after surgery, differs from the normal cartilage and probably lacks the distinctive collagen arrangement of native cartilage. According

to dGEMRIC, a varying degree of proteoglycan replenishment takes place. A combination of these two quantitative magnetic resonance imaging techniques permits a more comprehensive characterization of the degree of cartilage repair.

REFERENCES

[1] S. V. Akella, R. R. Regatte, A. J. Gougoutas, A. Borthakur, E. M. Shapiro, J. B. Kneeland, J. S. Leigh, and R. Reddy. Proteoglycan-induced changes in $T_{1\rho}$-relaxation of articular cartilage at 4T. *Magn Reson Med*, 46(3):419–423, 2001.

[2] S. Akizuki, V. C. Mow, F. Muller, J. C. Pita, D. S. Howell, and D. H. Manicourt. Tensile properties of human knee joint cartilage: I. Influence of ionic conditions, weight bearing, and fibrillation on the tensile modulus. *J Orthop Res*, 4(4):379–392., 1986.

[3] H. A. Alhadlaq, Y. Xia, F. M. Hansen, C. M. Les, and G. Lust. Morphological changes in articular cartilage due to static compression: polarized light microscopy study. *Connect Tissue Res*, 48(2):76–84, 2007.

[4] C. G. Armstrong and V. C. Mow. Variations in the intrinsic mechanical properties of human articular cartilage with age, degeneration, and water content. *J Bone Joint Surg Am*, 64(1):88–94, 1982.

[5] J. P. Arokoski, M. M. Hyttinen, T. Lapveteläinen, P. Takacs, B. Kosztaczky, L. Modis, V. Kovanen, and H. Helminen. Decreased birefringence of the superficial zone collagen network in the canine knee (stifle) articular cartilage after long distance running training, detected by quantitative polarised light microscopy. *Ann Rheum Dis*, 55(4):253–264., 1996.

[6] A. Aromaa and S. Koskinen. *Health and functional capacity in Finland. Baseline results of the Health 2000 health examination survey*. National Public Health Institute, Helsinki, 2002.

[7] K. A. Athanasiou, A. Agarwal, and F. J. Dzida. Comparative study of the intrinsic mechanical properties of the human acetabular and femoral head cartilage. *J Orthop Res*, 12(3):340–349, 1994.

[8] K. A. Athanasiou, M. P. Rosenwasser, J. A. Buckwalter, T. I. Malinin, and V. C. Mow. Interspecies comparisons of *in situ* intrinsic mechanical properties of distal femoral cartilage. *J Orthop Res*, 9(3):330–340, 1991.

[9] M. Baldassarri, J. S. Goodwin, M. L. Farley, B. E. Bierbaum, S. R. Goldring, M. B. Goldring, D. Burstein, and M. L. Gray. Relationship between cartilage stiffness and dGEMRIC index: correlation and prediction. *J Orthop Res*, 25(7):904–912, 2007.

[10] R. A. Bank, M. Soudry, A. Maroudas, J. Mizrahi, and J. M. TeKoppele. The increased swelling and instantaneous deformation of osteoarthritic cartilage is highly correlated with collagen degradation. *Arthritis Rheum*, 43(10):2202–2210, 2000.

[11] W. Bartlett, A. M. Flanagan, C. R. Gooding, R. W. J. Carrington, A. M. Flanagan, T. W. R. Briggs, and G. Bentley. Autologous chondrocyte implantation versus matrix-induced autologous chondrocyte implantation for osteochondral defects of the knee: A prospective, randomized study. *J Bone Joint Surg Br*, 87:640–645, 2005.

[12] A. Bashir, M. L. Gray, R. D. Boutin, and D. Burstein. Glycosaminoglycan in articular cartilage: Glycosaminoglycan in articular cartilage: *in vivo* assessment with delayed Gd-DTPA^{2-}-enhanced MR imaging. *Radiology*, 205(2):551–558, 1997.

[13] A. Bashir, M. L. Gray, and D. Burstein. Gd-DTPA^{2-} as a measure of cartilage degradation. *Magn Reson Med*, 36(5):665–673, 1996.

[14] A. Bashir, M. L. Gray, J. Hartke, and D. Burstein. Nondestructive imaging of human cartilage glycosaminoglycan concentration by MRI. *Magn Reson Med*, 41(5):857–865, 1999.

[15] P. J. Basser, J. Mattiello, and D. LeBihan. MR diffusion tensor spectroscopy and imaging. *Biophys J*, 66(1):259–267, 1994.

[16] M. Benjamin and G. M. Bydder. Magnetic resonance imaging of entheses using ultrashort TE (UTE) pulse sequences. *J Magn Reson Imaging*, 25(2):381–389, 2007.

[17] H. S. Bennett. Methods applicable to the study of both fresh and fixed materials. The microscopical investigation of biological materials with polarized light. In J.R. McClung, editor, *McClung's handbook of microscopical technique*, pages 591–677. Paul B Hoeber, New York, 1950.

[18] J. M. Bland and D. G. Altman. Statistical methods for assessing agreement between two methods of clinical measurement. *Lancet*, 1(8476):307–310, 1986.

[19] F. Bloch, W. W. Hansen, and M. E. Packard. Nuclear introduction. *Phys Rev*, 69:127, 1946.

[20] R. Bolbos, J. B. Benoit-Cattin, A. Langlois, A. Chomel, E. Chereul, C. Odet, P. Pastoureau, M. Janier, and O. Beuf. Knee cartilage thickness measurements using MRI: a 4 1/2-month longitudinal study in the meniscectomized guinea pig model of OA. *Osteoarthritis and Cartilage*, 15:656–665, 2007.

[21] A. Borthakur, E. Mellon, S. Niyogi, W. Witschey, J. B. Kneeland, and R. Reddy. Sodium and $T_{1\rho}$ MRI for molecular and diagnostic imaging of articular cartilage. *NMR Biomed*, 19:781–821, 2006.

[22] C. Boulocher, E. Chereul, J. B. Langlois, M. Armenean, M. E. Duclos, E. Viguier, T. Roger, and E. Vignon. Non-invasive *in vivo* quantification of the tibial cartilage thickness progression in an osteoarthritis rabbit model with quantitative 3D high resolution micro-MRI. *Osteoarthritis and Cartilage*, 15:in press, 2007.

[23] B. H. Brismar, T. Wredmark, T. Movin, J. Leandersson, and O. Svensson. Observer reability in the arthroscopic classification of osteoarthritis of the knee. *J Bone Joint Surg Br*, 84(1):42–47, 2002.

[24] M. Brittberg, A. Lindahl, A. Nilsson, C. Ohlsson, O. Isaksson, and L. Peterson. Treatment of deep cartilage defects in the knee with autologous chondrocyte transplantation. *N Engl J Med*, 331(14):889–895, 1994.

[25] R. Brocklehurst, M. T. Bayliss, A. Maroudas, H. L. Coysh, M. A. Freeman, P. A. Revell, and S. Y. Ali. The composition of normal and osteoarthritic articular cartilage from human knee joints. With special reference to unicompartmental replacement and osteotomy of the knee. *J Bone Joint Surg Am*, 66(1):95–106, 1984.

[26] R. G. Bryant. The dynamics of water-protein interactions. *Annu Rev Biophys Biomol Struct*, 25:29–53, 1996.

[27] J. A. Buckwalter and H. J. Mankin. Articular Cartilage, Part II: Degeneration and osteoarthrosis, repair, regeneration, and transplantation. *J Bone Joint Surg Am*, 79(4):612–632, 1997.

[28] J. A. Buckwalter, L. C. Rosenberg, and E. B. Hunziker. Articular cartilage: Composition, structure, response to injury, and methods of facilitating repair. In J. W. Ewing, editor, *Articular cartilage and knee joint function: Basic science and arthroscopy.*, pages 19–56. Raven Press, Ltd., New York, 1990.

[29] D. Burstein, J. Velyvis, K. T. Scott, K. W. Stock, Y. J. Kim, D. Jaramillo, R. D. Boutin, and M. L. Gray. Protocol issues for delayed Gd-DTPA^{2-}-enhanced MRI (dGEMRIC) for clinical evaluation of articular cartilage. *Magn Reson Med*, 45(1):36–41., 2001.

[30] M. D. Buschmann, J. Soulhat, A. Shirazi-Adl, J. S. Jurvelin, and E. B. Hunziker. Confined compression of articular cartilage: linearity in ramp and sinusoidal tests and the importance of interdigitation and incomplete confinement. *J Biomech*, 31(2):171–178, 1998.

[31] J. Choy, W. Ling, and A. Jerschow. Selective detection of ordered sodium signals via the central transition. *J Magn Reson*, 180:105–109, 2006.

[32] B. Cohen, W. M. Lai, and V. C. Mow. A transversely isotropic biphasic model for unconfined compression of growth plate and chondroepiphysis. *J Biomech Eng*, 120(4):491–496, 1998.

[33] T. Cunningham, R. Jessel, D. Zurakowski, M. B. Millis, and Y. J. Kim. Delayed gadolinium-enhanced magnetic resonance imaging of cartilage to predict early failure of Bernese periacetabular osteotomy for hip dysplasia. *J Bone Joint Surg Am*, 88(7):1540–1548, 2006.

[34] X. Deng, M. Farley, M. T. Nieminen, M. Gray, and D. Burstein. Diffusion tensor imaging of native and degenerated human articular cartilage. *Magn Reson Imag*, 25:168–171, 2007.

[35] C. Ding, F. Cicutti, L. Blizzard, F. Scott, and G. Jones. A longitudinal study of the effect of sex and age on rate of change in knee cartilage volume in adults. *Rheumatology*, 46:273–279, 2007.

[36] M. R. DiSilvestro and J. K. Suh. A cross-validation of the biphasic poroviscoelastic model of articular cartilage in unconfined compression, indentation, and confined compression. *J Biomech*, 34(4):519–525., 2001.

[37] M. R. DiSilvestro, Q. Zhu, M. Wong, J. S. Jurvelin, and J. K. Suh. Biphasic poroviscoelastic simulation of the unconfined compression of articular cartilage: I–simultaneous prediction of reaction force and lateral displacement. *J Biomech Eng*, 123(2):191–197, 2001.

[38] K. M. Donahue, D. Burstein, W. J. Manning, and M. L. Gray. Studies of Gd-DTPA relaxivity and proton exchange rates in tissue. *Magn Reson Med*, 32(1):66–76, 1994.

[39] J. Duryea, G. Neumann, M. H. Brem, W. Koh, F. Noorbakhsh, R. D. Jackson, J. Yu, C. B. Eaton, and P. Lang. Novel fast semi-automated software to segment cartilage for knee MR acquisitions. *Osteoarthritis Cartilage*, 15(5):487–492, 2007.

[40] U. Duvvuri, S. R. Charagundla, S. B. Kudchodkar, J. H. Kaufman, J. B. Kneeland, R. Rizi, J. S. Leigh, and R. Ravinder. Human knee-in vivo $T_{1\rho}$-weighted MR imaging at 1.5T-preliminary experience. *Radiology*, 220:822–826, 2001.

[41] U. Duvvuri, A. D. Goldberg, J. K. Kranz, L. Hoang, R. Reddy, F. W. Wehrli, A. J. Wand, S. W. Englander, and J. S. Leigh. Water magnetic relaxation dispersion in biological systems: the contribution of proton exchange and implications for the noninvasive detection of cartilage degradation. *Proc Natl Acad Sci U S A*, 98(22):12479–12484, 2001.

[42] R. B. Dzioba. The classification and treatment of acute articular cartilage lesions. *Arthroscopy*, 4(2):72–80, 1988.

[43] F. Eckstein, R. J. Buck, B. T. Wyman, J. J. Kotyk, M. P. Le Graverand, A. E. Remmers, J. L. Evelhoch, M. Hudelmaier, and H. C. Charles. Quantitative imaging of cartilage morphology at 3.0 Tesla in the presence of gadopentate dimeglumine (Gd-DTPA). *Magn Reson Med*, 58(2):402–406, 2007.

[44] F. Eckstein, D. Burstein, and TM. Link. Quantitative MRI of cartilage and bone: degenerative changes in osteoarthritis. *NMR Biomed*, 19:822–854, 2006.

[45] F. Eckstein, J. Westhoff, H. Sittek, K. P. Maag, M. Haubner, S. Faber, K. H. Englmeier, and M. Reiser. *In vivo* reproducibility of three-dimensional cartilage volume and thickness measurements with MR imaging. *AJR Am J Roentgenol*, 170(3):593–597, 1998.

[46] J. J. Elias and A. J. Cosgarea. Computational modeling: an alternative approach for investigating patellofemoral mechanics. *Sports Med Arthrosc*, 15(2):89–94, 2007.

[47] A. Engel. MR -knee imaging. *Acta Orthop scan Suppl*, 61:1–57, 1990.

[48] L. V. Engelhardt, C. N. Kraft, P. H. Pennekamp, H. H. Schild, A. Schmitz, and M. Falkenhausen. The evaluation of articular cartilage lesions of the knee with a 3- Tesla magnet. *Arthroscopy*, 23:496–502, 2007.

[49] D. Figueroa, R. Calco, A. Vaisman, M. A. Carrasco, C. Moraga, and I. Delgado. Knee chondral lesions: incidence and correlation between arthroscopic and magnetic resonance findings. *Arthroscopy*, 23:312–315, 2007.

[50] L. Filidoro, O. Dietrich, J. Weber, E. Rauch, T. Oerther, M. Wick, M. F. Reiser, and C. Glaser. High-resolution diffusion tensor imaging of human patellar cartilage: feasibility and preliminary findings. *Magn Reson Med*, 53(5):993–998, 2005.

[51] K. W. Fishbein, H. C. Canuto, P. Bajaj, N. P. Camacho, and R. G. Spencer. Optimal methods of the preservation of cartilage samples in MRI and correlative biochemical studies. *Magn Reson Med*, 57:866–873, 2007.

[52] M. Fortin, J. Soulhat, A. Shirazi-Adl, E. B. Hunziker, and M. D. Buschmann. Unconfined compression of articular cartilage: nonlinear behavior and comparison with a fibril-reinforced biphasic model. *J Biomech Eng*, 122(2):189–195, 2000.

[53] D. M. Freeman, G. Bergman, and G. Glover. Short TE MR microscopy: accurate measurement and zonal differentiation of normal hyaline cartilage. *Magn Reson Med*, 38(1):72–81, 1997.

[54] G. D. Fullerton. Physiologic basis of magnetic relaxation. In D.D. Stark and W.G. Bradley, editors, *Magnetic resonance imaging*, pages 36–54. Bradley, Baltimore, 1992.

[55] A. Gillis, A. Bashir, B. McKeon, A. Scheller, M. L. Gray, and D. Burstein. Magnetic resonance imaging of relative glycosaminoglycan distribution in patients with autologous chondrocyte transplants. *Invest Radiol*, 36(12):743–748, 2001.

[56] C. Glaser, S. Faber, F. Eckstein, H. Fischer, V. Springer, L. Heudorfer, T. Stammberger, K. H. Engelmeier, and M. Reiser. Optimization and validation of rapid high-resolution T1-w 3D flash water excitation MRI sequence for the quantitative assessment of articular cartilage volume and thickness. *Magn Reson Imag*, 19:177–185, 2001.

[57] C. Glaser, B. J. Tins, C. G. Trumm, J. B. Richardson, M. F. Reiser, and I. W. McCall. Quantitative 3D MR evaluation of autologous chondrocyte implantation in the knee: feasibility and initial results. *Osteoarthritis and Cartilage*, 15:798–807, 2007.

[58] C. C. Glüer, G. Blake, Y. Lu, B. A. Blunt, M. Jergas, and H. K. Genant. Accurate assessment of precision errors: how to measure the reproducibility of bone densitometry techniques. *Osteoporos Int*, 5(4):262–270, 1995.

[59] D. W. Goodwin, Y. Z. Wadghiri, and J. F. Dunn. Micro-imaging of articular cartilage: T_2, proton density, and the magic angle effect. *Acad Radiol*, 5(11):790–798, 1998.

[60] D. W. Goodwin, H. Zhu, and J. F. Dunn. *In vitro* MR imaging of hyaline cartilage: correlation with scanning electron microscopy. *AJR Am J Roentgenol*, 174(2):405–409, 2000.

[61] D. A. Grande, I. J. Singh, and J. Pugh. Healing of experimentally produced lesions in articular cartilage following chondrocyte transplantation. *Anat Rec*, 218(2):142–148, 1987.

[62] M. L. Gray, D. Burstein, Y. J. Kim, and A. Maroudas. Magnetic resonance imaging of cartilage glycosaminoglycan: Basic principles, imaging technique, and clinical applications. *J Orthop Res*, 26(3):281–291, 2008.

[63] M. L. Gray, D. Burstein, L. M. Lesperance, and Gehrke Lee. Magnetization transfer in cartilage and its constituent macromolecules. *Magnetic Resonance in Medicine*, 34(3):319–325, 1995.

[64] W. Gründer, M. Kanowski, M. Wagner, and A. Werner. Visualization of pressure distribution within loaded joint cartilage by application

of angle-sensitive NMR microscopy. *Magn Reson Med*, 43(6):884–891., 2000.

[65] W. Gründer, M. Wagner, and A. Werner. MR-microscopic visualization of anisotropic internal cartilage structures using the magic angle technique. *Magn Reson Med*, 39(3):376–382, 1998.

[66] A. J. Grodzinsky. Electromechanical and physicochemical properties of connective tissue. *Crit Rev Biomed Eng*, 9(2):133–199, 1983.

[67] A. E. Gross. Fresh osteochondral allografts for post-traumatic knee defects: surgical technique. *Operative Techniques in Orthopaedics*, 7(4):334–339, 1997.

[68] W. Y. Gu, W. M. Lai, and V. C. Mow. Transport of fluid and ions through a porous-permeable charged-hydrate tissue, and streaming potential data on normal bovine articular cartilage. *J Biomech*, 26:709–723, 1993.

[69] W. Y. Gu, W. M. Lai, and V. C. Mow. A triphasic analysis of negative osmotic flows through charged hydrated soft tissues. *J Biomech*, 30(1):71–78, 1997.

[70] WY. Gu, WM. Lai, and VC. Mow. A mixture theory for charged-hydrated soft tissues containing multi- electrolytes: passive transport and swelling behaviors. *J Biomech Eng*, 120(2):169–180, 1998.

[71] E. M. Haacke, R. W. Brown, M.R. Thompson, and R. Venkatesan. *Magnetic Resonance Imaging: physical principles and sequence design*. Wiley-Liss, New York, 1999.

[72] L. Hangody and P. Fules. Autologous osteochondral mosaicplasty for the treatment of full-thickness defects of weight-bearing joints: ten years of experimental and clinical experience. *J Bone Joint Surg Am*, 85-A(Suppl 2):25–32, 2003.

[73] L. Hangody, G. Kish, Z. Karpati, I. Szerb, and I. Udvarhelyi. Arthroscopic autogenous osteochondral mosaicplasty for the treatment of femoral condylar articular defects. a preliminary report. *Knee Surg Sports Traumatol Arthrosc*, 5:262–267, 1997.

[74] I. Hannila, M. T. Nieminen, E. Rauvala, O. Tervonen, and R. Ojala. Patellar cartilage lesions: comparison of magnetic resonance imaging and T_2 relaxation-time mapping. *Acta Radiologica*, 48:444–448, 2007.

[75] W. C. Hayes, L. M. Keer, G. Herrmann, and L. F. Mockros. A mathematical analysis for indentation tests of articular cartilage. *J Biomech*, 5(5):541–551, 1972.

[76] I. Henderson, P. Lavigne, H. Valenzuela, and B. Oakes. Autologous chondrocyte implantation: superior biologic properties of hyaline cartilage repairs. *Clin Orthop Relat Res*, 455:253–261, 2007.

[77] R. M. Henkelman, G. J. Stanisz, J. K. Kim, and M. J. Bronskill. Anisotropy of NMR properties of tissues. *Magn Reson Med*, 32(5):592–601, 1994.

[78] V. E. Hoikka, H. J. Jaroma, and V. A. Ritsilä. Reconstruction of the patellar articulation with periosteal grafts. *Acta Orthop Scand*, 61:36–39, 1990.

[79] D. Hopwood. Fixation and fixatives. In J.D. Bancroft and A. Stevens, editors, *Theory and Practice of Histological Techiniques*, pages 16–28. Churchill Livingstone, London, 1977.

[80] D. J. Hunter, J. Niu, Y. Zhang, M. Lavalley, C. E. McClennan, M. Hudelmaier, F. Eckstein, and D. T. Felson. Premorbid knee OA is not characterized by diffuse thinness: The Framingham study. *Ann Rheum Dis*, Epub ahead of print, 2008.

[81] E. B. Hunziker, E. Kapfinger, and J. Geiss. The structural architecture of adult mammalian articular cartilage evolves by a synchronized process of tissue resorption and neoformation during postnatal development. *Osteoarthritis Cartilage*, 15(4):403–413, 2007.

[82] E. B. Hunziker, T. M. Quinn, and H. J. Häuselmann. Quantitative structural organization of normal adult human articular cartilage. *Osteoarthritis Cartilage*, 10(7):564–572, 2002.

[83] W. R. Inch, J. A. McCredie, C. Geiger, and Y. Boctor. Spin-lattice relaxation times for mixtures of water and gelatin or cotton, compared with normal and malignant tissue. *J Natl Cancer Inst*, 53(3):689–690, 1974.

[84] W. R. Inch, J. A. McCredie, R. R. Knispel, R. T. Thompson, and M. M. Pintar. Water content and proton spin relaxation time for neoplastic and non-neoplastic tissues from mice and humans. *J Natl Cancer Inst*, 52(2):353–356, 1974.

[85] J. L. Jaremko, C. M. Maciejewski, R. W. Cheng, J. L. Ronsky, R. B. Thompson, R. G. Lambert, and S. S. Dhillon. Accuracy and reliability of MRI vs. laboratory measurements in an *ex vivo* porcine model of arthritic cartilage loss. *J Magn Reson Imaging*, 26(4):992–1000, 2007.

[86] J. S. Jurvelin, J. P. Arokoski, E. B. Hunziker, and H. J. Helminen. Topographical variation of the elastic properties of articular cartilage in the canine knee. *J Biomech*, 33(6):669–675, 2000.

[87] J. S. Jurvelin, M. D. Buschmann, and E. B. Hunziker. Mechanical anisotropy of the human knee articular cartilage in compression. *Proc Inst Mech Eng [H]*, 217(3):215–219, 2003.

[88] K. Keinan-Adamsky, H. Shinar, and G. Navon. The effect of decalcification on the microstructure of articular cartilage assessed by ^{2}H double quantum filtered spectroscopic MRI. *Magma*, 18(5):231–237, 2005.

[89] K. Keinan-Adamsky, H. Shinar, and G. Navon. Multinuclear NMR and MRI studies of the maturation of pig articular cartilage. *Magn Reson Med*, 55(3):532–540, 2006.

[90] P. S. Khalsa and S. R. Eisenberg. Compressive behavior of articular cartilage is not completely explained by proteoglycan osmotic pressure. *J Biomech*, 30(6):589–594., 1997.

[91] Y. J. Kim, D. Jaramillo, M. B. Millis, M. L. Gray, and D. Burstein. Assessment of early osteoarthritis in hip dysplasia with delayed gadolinium-enhanced magnetic resonance imaging of cartilage. *J Bone Joint Surg Am*, 85-A(10):1987–1992, 2003.

[92] K. Király, T. Lapveteläinen, J. Arokoski, K. Törrönen, L. Modis, I. Kiviranta, and H. J. Helminen. Application of selected cationic dyes for the semiquantitative estimation of glycosaminoglycans in histological sections of articular cartilage by microspectrophotometry. *Histochem J*, 28(8):577–590., 1996.

[93] I. Kiviranta, J. Jurvelin, M. Tammi, A. M. Säämänen, and H. J. Helminen. Microspectrophotometric quantitation of glycosaminoglycans in articular cartilage sections stained with Safranin O. *Histochemistry*, 82(3):249–255, 1985.

[94] S. Koo, G. E. Gold, and T. P. Andriacchi. Considerations in measuring cartilage thickness using MRI: factors influencing reproducibility and accuracy. *Osteoarthritis Cartilage*, 13(9):782–789, 2005.

[95] R. K. Korhonen, M. S. Laasanen, J. Toyras, R. Lappalainen, H. J. Helminen, and J. S. Jurvelin. Fibril reinforced poroelastic model predicts specifically mechanical behavior of normal, proteoglycan depleted and collagen degraded articular cartilage. *J Biomech*, 36(9):1373–1379, 2003.

[96] R. K. Korhonen, M. S. Laasanen, J. Töyräs, H. J. Helminen, and J. S. Jurvelin. Comparison of the equilibrium response of articular cartilage in unconfined compression, confined compression and indentation. *J Biomech*, 35(7):903–909, 2002.

[97] R. K. Korhonen, M. Wong, J. Arokoski, R. Lindgren, H. J. Helminen, E. B. Hunziker, and J. S. Jurvelin. Importance of the superficial tissue layer for the indentation stiffness of articular cartilage. *Med Eng Phys*, 24(2):99–108, 2002.

[98] M. S. Laasanen, J. Toyras, R. K. Korhonen, J. Rieppo, S. Saarakkala, M. T. Nieminen, J. Hirvonen, and J. S. Jurvelin. Biomechanical properties of knee articular cartilage. *Biorheology*, 40(1-3):133–140, 2003.

[99] E. Lammentausta, P. Kiviranta, M. J. Nissi, M. S. Laasanen, I. Kiviranta, M. T. Nieminen, and J. S. Jurvelin. T_2 relaxation time and delayed gadolinium-enhanced MRI of cartilage (dGEMRIC) of human patellar cartilage at 1.5 T and 9.4 T: Relationships with tissue mechanical properties. *J Orthop Res*, 24(3):366–374, 2006.

[100] D. Laurent, J. Wasvary, J. Yin, M. Rubin, T. C. Pellas, and E. O'Byrne. Quantitative and qualitative assessment of articular cartilage in the goat knee with magnetization transfer imaging. *Magn Reson Imaging*, 19:1279–1286, 2001.

[101] T. Laurent, J. Wasvary, M. Rudin, E. O'Byrne, and T. Pellas. *In vivo* assessment of macromolecular content in articular cartilage of the goat knee. *Magn Reson Med*, 49:1037–1046, 2003.

[102] K. Y. Lee, T. C. Dunn, L. S. Steinbach, E. Ozhinsky, M. D. Ries, and S. Majumdar. Computer-aided quantification of focal cartilage lesions of osteoarthritic knee using MRI. *Magn Reson Imaging*, 22(8):1105–1115, 2004.

[103] R. C. Lee, E. H. Frank, A. J. Grodzinsky, and D. K. Roylance. Oscillatory compressional behavior of articular cartilage and its associated electromechanical properties. *J Biomech Eng*, 103(4):280–292, 1981.

[104] G. Li, S. E. Park, L. E. DeFrate, M. E. Schutzer, L. Ji, T. J. Gill, and H. E. Rubash. The cartilage thickness distribution in the tibiofemoral joint and its correlation with cartilage-to-cartilage contact. *Clin Biomech*, 20:736–744, 2005.

[105] X. Li, C. Benjamin Ma, T. M. Link, D. D. Castillo, B. S. Blumenkrantz, J. Lozano, J. Carballido-Gamio, M. Ries, and S. Majumdar. *In vivo* $T_{1\rho}$ and T_2 mapping of articular cartilage in osteoarthritis of the knee using 3T MRI. *Osteoarthritis and Cartilage*, 15:789–797, 2007.

[106] C. Liess, S. Lusse, N. Karger, M. Heller, and C.-C. Gluer. Detection of changes in cartilage water content using MRI T_2-mapping *in vivo*. *Osteoarthritis and Cartilage*, 10(12):907–913, 2002.

[107] W. Ling, R. R. Regatte, G. Navon, and A. Jerschow. Assessment of glycosaminoglycan concentration *in vivo* by chemical exchange-dependent saturation transfer (gagCEST). *Proc Natl Acad Sci U S A*, 105(7):2266–2270, 2008.

[108] W. Ling, R. R. Regatte, M. E. Schweizer, and A. Jerschow. Behaviour of ordered sodium in enzymatically depleted cartilage tissue. *Magn Reson Med*, 56:1151–1155, 2006.

[109] S. Lüsse, H. Claassen, T. Gehrke, J. Hassenpflug, M. Schunke, M. Heller, and C. C. Gluer. Evaluation of water content by spatially resolved transverse relaxation times of human articular cartilage. *Magn Reson Imaging*, 18(4):423–430, 2000.

[110] T. Lyyra, I. Kiviranta, U. Vaatainen, H. J. Helminen, and J. S. Jurvelin. *In vivo* characterization of indentation stiffness of articular cartilage in the normal human knee. *J Biomed Mater Res*, 48(4):482–487, 1999.

[111] C. F. Maier, S. G. Tan, H. Hariharan, and H. G. Potter. T_2 quantitation of articular cartilage at 1.5 T. *J Magn Reson Imaging*, 17:358–364, 2003.

[112] A. F. Mak. The apparent viscoelastic behavior of articular cartilage–the contributions from the intrinsic matrix viscoelasticity and interstitial fluid flows. *J Biomech Eng*, 108(2):123–130, 1986.

[113] H. J. Mankin and A. Z. Thrasher. Water content and binding in normal and osteoarthritic human cartilage. *J Bone Joint Surg Am*, 57(1):76–80., 1975.

[114] A. Maroudas and R. Schneiderman. "Free" and "exchangeable" or "trapped" and "non-exchangeable" water in cartilage. *J Orthop Res*, 5:133–138, 1987.

[115] C. A. McKenzie, A. Williams, P. V. Prasad, and D. Burstein. Three-dimensional delayed gadolinium-enhanced MRI of cartilage (dGEMRIC) at 1.5T and 3.0T. *J Magn Reson Imaging*, 24:928–933, 2006.

[116] R. Meder, S. K. de Visser, J. C. Bowden, T. Bostrom, and J. M. Pope. Diffusion tensor imaging of articular cartilage as a measure of tissue microstructure. *Osteoarthritis Cartilage*, 14(9):875–881, 2006.

[117] T. Mendlik, S. C. Faber, J. Weber, J. Hohe, E. Rauch, M. Reiser, and C. Glaser. T_2 quantitation of human articular cartilage in a clinical setting at 1.5 T: implementation and testing of four multiecho pulse sequence designs for validity. *Invest Radiol*, 39(5):288–299, 2004.

[118] N. M. Menezes, M. L. Gray, J. R. Hartke, and D. Burstein. T_2 and $T_{1\rho}$ MRI in articular cartilage systems. *Magn Reson Med*, 51(3):503–509, 2004.

[119] T. Minas and L. Peterson. Advanced techniques in autologous chondrocyte transplantation. *Clin Sports Med*, 18(1):13–44, v–vi, 1999.

[120] S. Miyata, T. Numano, K. Homma, T. Tateishi, and T. Ushida. Feasibility of noninvasive evaluation of biophysical properties of tissue-engineered cartilage by using quantitative MRI. *J Biomech*, 40(13):2990–2998, 2007.

[121] J. Mizrahi, A. Maroudas, Y. Lanir, I. Ziv, and T. J. Webber. The "instantaneous" deformation of cartilage: effects of collagen fiber orientation and osmotic stress. *Biorheology*, 23:311–330, 1986.

[122] V. Mlynárik, A. Degrassi, R. Toffanin, F. Vittur, M. Cova, and R. S. Pozzi-Mucelli. Investigation of laminar appearance of articular cartilage by means of magnetic resonance microscopy. *Magn Reson Imaging*, 14(4):435–442, 1996.

[123] V. Mlynárik, I. Sulzbacher, M. Bittsansky, R. Fuiko, and S. Trattnig. Investigation of apparent diffusion constant as an indicator of early degenerative disease in articular cartilage. *J Magn Reson Imaging*, 17:440–444, 2003.

[124] V. Mlynárik, P. Szomolanyi, R. Toffanin, F. Vittur, and S. Trattnig. Transverse relaxation mechanisms in articular cartilage. *J Magn Reson*, 169(2):300–307, 2004.

[125] V. Mlynárik, S. Trattnig, M. Huber, A. Zembsch, and H. Imhof. The role of relaxation times in monitoring proteoglycan depletion in articular cartilage. *J Magn Reson Imaging*, 10(4):497–502., 1999.

[126] T. J. Mosher and B. J. Dardzinski. Cartilage MRI T_2 relaxation time mapping: overview and applications. *Semin Musculoskelet Radiol*, 8(4):355–368, 2004.

[127] T. J. Mosher, H. Smith, B. J. Dardzinski, V. J. Schmithorst, and M. B. Smith. MR imaging and T_2 mapping of femoral cartilage: *in vivo* determination of the magic angle effect. *Am J Roentgenol*, 177(3):665–669, 2001.

[128] V. C. Mow, S. C. Kuei, W. M. Lai, and C. G. Armstrong. Biphasic creep and stress relaxation of articular cartilage in compression: Theory and experiments. *J Biomech Eng*, 102(1):73–84, 1980.

[129] V. C. Mow, A. Ratcliffe, and A. R. Poole. Cartilage and diarthrodial joints as paradigms for hierarchical materials and structures. *Biomaterials*, 13(2):67–97, 1992.

[130] V. C. Mow, W. Zhu, and A. Ratcliffe. Structure and function of articular cartilage and meniscus. In V. C. Mow and W. C. Hayes, editors, *Basic orthopaedic biomechanics*, pages 143–198. Raven Press, Ltd, New York, 1991.

[131] G. Navon, H. Shinar, U. Eliav, and Y. Seo. Multiquantum filters and order in tissues. *NMR Biomed*, 14(2):112–132, 2001.

[132] M. T. Nieminen, N. M. Menezes, A. Williams, and D. Burstein. T_2 of articular cartilage in the presence of Gd-DTPA^{2-}. *Magn Reson Med*, 51(6):1147–1152, 2004.

[133] M. T. Nieminen, J. Rieppo, J. Silvennoinen, J. Töyräs, J. M. Hakumäki, M. M. Hyttinen, H. J. Helminen, and J. S. Jurvelin. Spatial assessment of articular cartilage proteoglycans with Gd-DTPA -enhanced T_1 imaging. *Magn Reson Med*, 48(4):640–648, 2002.

[134] M. T. Nieminen, J. Rieppo, J. Töyräs, J. M. Hakumäki, M. J. Silvennoinen, M. M. Hyttinen, H. J. Helminen, and J. S. Jurvelin. T_2 relaxation reveals spatial collagen architecture in articular cartilage: a comparative quantitative MRI and polarized light microscopic study. *Magn Reson Med*, 46(3):487–493, 2001.

[135] M. T. Nieminen, J. Töyräs, M. S. Laasanen, J. Silvennoinen, H. J. Helminen, and J. S. Jurvelin. Prediction of biomechanical properties of articular cartilage with quantitative magnetic resonance imaging. *J Biomech*, 37(3):321–328, 2004.

[136] M. T. Nieminen, J. Töyräs, J. Rieppo, J. M. Hakumäki, J. Silvennoinen, H. J. Helminen, and J. S. Jurvelin. Quantitative MR microscopy of enzymatically degraded articular cartilage. *Magn Reson Med*, 43(5):676–681, 2000.

[137] M. J. Nissi, J. Rieppo, J. Toyras, M. S. Laasanen, I. Kiviranta, J. S. Jurvelin, and M. T. Nieminen. T_2 relaxation time mapping reveals age- and species-related diversity of collagen network architecture in articular cartilage. *Osteoarthritis Cartilage*, 14(12):1265–1271, 2006.

[138] M. J. Nissi, J. Töyräs, M. S. Laasanen, J. Rieppo, S. Saarakkala, R. Lappalainen, J. S. Jurvelin, and M. T. Nieminen. Proteoglycan and collagen sensitive MRI evaluation of normal and degenerated articular cartilage. *J Orthop Res*, 22:557–564, 2004.

[139] S. W. O'Driscoll. Articular cartilage regeneration using periosteum. *Clin Orthop*, -(367 Suppl):S186–203, 1999.

[140] P. Olivier, D. Loeuille, A. Watrin, F. Walter, S. Etienne, P. Netter, P. Gillet, and A. Blum. Structural evaluation of articular cartilage: potential contribution of magnetic resonance techniques used in clinical practice. *Arthritis Rheum*, 44(10):2285–2295., 2001.

[141] S. F. Othman, J. Li, O. Abdullah, J. J. Moinnes, R. L. Magin, and C. Muehleman. High-resolution/high-contrast MRI of human articular cartilage lesions. *Acta Orthop*, 78(4):536–546, 2007.

[142] I. G. Otterness and F. Eckstein. Women have thinner cartilage and smaller joint surfaces than men after adjustment for body height and weight. *Osteoarthritis Cartilage*, 15(6):666–672, 2007.

[143] I. G. Otterness, M. P. Le Graverand, and F. Eckstein. Allometric relationships between knee cartilage volume, thickness, surface area and body dimensions. *Osteoarthritis Cartilage*, 16(1):34–40, 2008.

[144] S. K. Pakin, M. E. Schweitzer, and R. R. Regatte. 3D-$T_{1\rho}$ quantitation of patellar cartilage at 3.0T. *J Magn Reson Imaging*, 24:1357–1363, 2006.

[145] H. E. Panula, M. M. Hyttinen, J. P. A. Arokoski, T. K. Långsjö, A. Pelttari, I. Kiviranta, and H. J. Helminen. Articular cartilage superficial zone collagen birefringence reduced and cartilage thickness increased before surface fibrillation in experimental osteoarthritis. *Ann Rheum Dis*, 57(4):237–245, 1998.

[146] L. Peterson, M. Brittberg, I. Kiviranta, E. L. Åkerlund, and A. Lindahl. Autologous chondrocyte transplantation. Biomechanics and long-term durability. *Am J Sports Med*, 30:2–12, 2002.

[147] L. Peterson, T. Minas, M. Brittberg, A. Nilsson, E. Sjogren-Jansson, and A. Lindahl. Two- to 9-year outcome after autologous chondrocyte transplantation of the knee. *Clin Orthop*, -(374):212–234, 2000.

[148] A. R. Poole, T. Kojima, T. Yasuda, F. Mwale, M. Kobayashi, and S. Laverty. Composition and structure of articular cartilage: a template for tissue repair. *Clin Orthop*, -(391 Suppl):S26–33, 2001.

[149] E. L. Radin, I. L. Paul, and M. Lowy. A comparison of the dynamic force transmitting properties of subchondral bone and articular cartilage. *J Bone Joint Surg Am*, 52(3):444–456, 1970.

[150] R. R. Regatte, S. V. Akella, A. Borthakur, J. B. Kneeland, and R. Reddy. Proteoglycan depletion-induced changes in transverse relaxation maps of cartilage: comparison of T_2 and $T_{1\rho}$. *Acad Radiol*, 9(12):1388–1394, 2002.

[151] R. R. Regatte, S. V. Akella, A. J. Wheaton, G. Lech, A. Borthakur, J. B. Kneeland, and R. Reddy. 3D-$T_{1\rho}$-relaxation mapping of articular cartilage: *in vivo* assessment of early degenerative changes in symptomatic osteoarthritic subjects. *Acad Radiol*, 11(7):741–749, 2004.

[152] R. R. Regatte, S.V.S. Akella, A. Borthakur, J. B. Kneeland, and R. Reddy. *In vivo* proton MR three-dimensional $T_{1\rho}$ mapping of human articular cartilage: Initial experience. *Radiology*, 229:269–274, 2003.

[153] J. Rieppo, M. M. Hyttinen, R. Lappalainen, J. S. Jurvelin, and H. J. Helminen. Spatial determination of water, collagen and proteoglycan contents by Fourier transform infrared imaging and digital densitometry. *Transact Orthop Res Soc*, 29:1021, 2004.

[154] V. A. Ritsilä, S. Santavirta, S. Alhopuro, M. Poussa, H. Jaroma, J. M. Rubak, A. Eskola, V. Hoikka, O. Snellman, and K. Osterman. Periosteal and perichondral grafting in reconstructive surgery. *Clin Orthop Relat Res*, -(302):259–265, 1994.

[155] S. Roberts, A. P. Hollander, B. Caterson, J. Menage, and J. B. Richardson. Matrix turnover in human cartilage repair tissue in autologous chondrocyte implantation. *Arthritis Rheum*, 44:2586–2598, 2001.

[156] E. M. Roos and L. Dahlberg. Positive effects of moderate exercise on glycosaminoglycan content in knee cartilage: a four-month, randomized, controlled trial in patients at risk of osteoarthritis. *Arthritis Rheum*, 52(11):3507–3514, 2005.

[157] A. Ruano-Ravina and M. Jato Diaz. Autologous chondrocyte implantation: a systematic review. *Osteoarthritis Cartilage*, 14(1):47–51, 2006.

[158] J. D. Rubenstein, J. K. Kim, I. Morova-Protzner, P. L. Stanchev, and R. M. Henkelman. Effects of collagen orientation on MR imaging characteristics of bovine articular cartilage. *Radiology*, 188(1):219–226, 1993.

[159] J. T. Samosky, D. Burstein, W. Eric Grimson, R. Howe, S. Martin, and M. L. Gray. Spatially-localized correlation of dGEMRIC-measured GAG distribution and mechanical stiffness in the human tibial plateau. *J Orthop Res*, 23(1):93–101, 2005.

[160] G. S. Seo, J. Aoki, H. Moriya, O. Karakida, S. Sone, H. Hidaka, and T. Katsuyama. Hyaline cartilage: *in vivo* and *in vitro* assessment with magnetization transfer imaging. *Radiology*, 201:525–530, 1996.

[161] E. M. Shapiro, A. Borthakur, A. Gougoutas, and R. Reddy. ^{23}Na MRI accurately measures fixed charge density in articular cartilage. *Magn Reson Med*, 47(2):284–291, 2002.

[162] E. M. Shapiro, A. Borthakur, J. H. Kaufman, J. S. Leigh, and R. Reddy. Water distribution patterns inside bovine articular cartilage as visualized by ^{1}H magnetic resonance imaging. *Osteoarthritis Cartilage*, 9(6):533–538, 2001.

[163] H. Shinar and G. Navon. Multinuclear NMR and microscopic MRI studies of the articular cartilage nanostructure. *NMR Biomed*, 19:877–893, 2006.

[164] H. Shinar, Y. Seo, K. Ikoma, Y. Kusaka, U. Eliav, and G. Navon. Mapping the fiber orientation in articular cartilage at rest and under pressure studied by ^{2}H double quantum filtered MRI. *Magn Reson Med*, 48:322–330., 2002.

[165] B. Shuter, S. C. Wang, J. Roche, G. Briggs, and J. M. Pope. Relaxivity of Gd-EOB-DTPA in the normal and biliary obstructed guinea pig. *J Magn Reson Imaging*, 8(4):853–861., 1998.

[166] W. H. Simon. Scale effects in animal joints. I. Articular cartilage thickness and compressive stress. *Arthritis Rheum*, 13:244–256, 1970.

[167] R. Stahl, B. S. Blmenkrantz, J. Carballido-Gamio, S. Zhao, T. Munoz, H. Le Graverand-Gastineau, S. Majumdar, and T. M. Link. MRI-derived T_2 relaxation times and cartilage morphometry of the tibio-demoral joint in subjects with and without osteoarthritis during a 1-year follow-up. *Osteoarthritis and Cartilage*, in press, 2007.

[168] G. J. Stanisz and R. M. Henkelman. Gd-DTPA relaxivity depends on macromolecular content. *Magn Reson Med*, 44(5):665–667, 2000.

[169] J. R. Steadman, K. K. Briggs, J. J. Rodrigo, M. S. Kocher, T. J. Gill, and W. G. Rodkey. Outcomes of microfracture for traumatic chondral defects of the knee: average 11-year follow-up. *Arthroscopy*, 19(5):477–484, 2003.

[170] D. Studer, M. Chiquet, and E. B. Hunziker. Evidence for a distinct water-rich layer surrounding collagen fibrils in articular cartilage extracellular matrix. *J Struct Biol*, 117(2):81–85, 1996.

[171] D. D. Sun, X. E. Guo, M. Likhitpanichkul, W. M. Lai, and V. C. Mow. The influence of the fixed negative charges on mechanical and electrical behaviors of articular cartilage under unconfined compression. *J Biomech Eng*, 126:6–16, 2004.

[172] C. J. Tiderius, R. Jessel, Y. J. Kim, and D. Burstein. Hip dGEMRIC in asymptomatic volunteers and patients with early osteoarthritis: the influence of timing after contrast injection. *Magn Reson Med*, 57(4):803–805, 2007.

[173] C. J. Tiderius, L. E. Olsson, H. de Verdier, P. Leander, O. Ekberg, and L. Dahlberg. Gd-DTPA^{2-}-enhanced MRI of femoral knee cartilage: a dose-response study in healthy volunteers. *Magn Reson Med*, 46(6):1067–1071, 2001.

[174] A. J. Tins, I. W. McCall, T. Takahashi, V. Cassar-Pullicino, S. Roberts, B. Ashton, P. Richardson, and J. Richardson. Autologous chondrocyte implantation in knee joint: MR imaging and histologic features at 1-year follow-up. *Radiology*, 234(2):501–508, 2005.

[175] R. Toffanin, V. Mlynárik, S. Russo, P. Szomolanyi, A. Piras, and F. Vittur. Proteoglycan depletion and magnetic resonance parameters of articular cartilage. *Arch Biochem Biophys*, 390(2):235–242, 2001.

[176] S. Trattnig, M. Huber, M. J. Breitenseher, H. J. Trnka, T. Rand, A. Kaider, T. Helbich, H. Imhof, and D. Resnick. Imaging articular cartilage defects with 3D fat-suppressed echo planar imaging: comparison with conventional 3D fat-suppressed gradient echo sequence and correlation with histology. *J Comput Assist Tomogr*, 22(1):8–14, 1998.

[177] S. Trattnig, T. C. Mamisch, G. H. Welsch, C. Glaser, P. Szomolanyi, S. Gebetsroither, O. Stastny, W. Horger, S. Millington, and S. Marlovits. Quantitative T_2 mapping of matrix-associated autologous chondrocyte transplantation at 3 Tesla: an *in vivo* cross-sectional study. *Invest Radiol*, 42(6):442–448, 2007.

[178] S. Trattnig, S. A. Millington, P. Szomolanyi, and S. Marlovits. MR imaging of osteochondral grafts and autologous chondrocyte implantation. *Eur Radiol*, 17(1):103–118, 2007.

[179] S. Trattnig, V. Mlynárik, M. Breitenseher, M. Huber, A. Zembsch, T. Rand, and H. Imhof. MRI visualization of proteoglycan depletion

in articular cartilage via intravenous administration of Gd-DTPA. *Magn Reson Imaging*, 17(4):577–583, 1999.

[180] S. Trattnig, K. Pinker, C. Krestan, C. Plank, S. Millington, and S. Marlovits. Matrix-based autologous chondrocyte implantation for cartilage repair with HyalograftC: two-year follow-up by magnetic resonance imaging. *Eur J Radiol*, 57(1):9–15, 2006.

[181] D. J. Tyler, M. D. Robson, R. M. Henkelman, I. R. Young, and G. M. Bydder. Magnetic resonance imaging with ultrashort TE (UTE) PULSE sequences: technical considerations. *J Magn Reson Imaging*, 25(2):279–289, 2007.

[182] M. Uhl, A. Lahm, T. A. Bley, J. Haberstroh, E. Mrosek, N. Ghanem, and C. Erggelet. Experimental autologous osteochondral plug transfer in the treatment of focal chondral defects: magnetic resonance imaging signs of technical success in sheep. *Acta Radiologica*, 47:875–880, 2005.

[183] I. Van Breuseghem, F. Palmieri, R. R. Peeters, F. Maes, H. T. Bosmans, and G. J. Marchal. Combined T_1-T_2 mapping of human femoro-tibial cartilage with turbo-mixed imaging at 1.5T. *J Magn Reson Imaging*, 22(3):368–372, 2005.

[184] A. I. Vasara, M. T. Nieminen, J. S. Jurvelin, L. Peterson, A. Lindahl, and I. Kiviranta. Indentation stiffness of repair tissue after autologous chondrocyte transplantation. In *Clin Orthop Relat Res*, pages 233–242, 2005.

[185] L. Wachsmuth, H. P. Juretschke, and R. X. Raiss. Can magnetization transfer magnetic resonance imaging follow proteoglycan depletion in articular cartilage? *Magma*, 5:71–78, 1997.

[186] C. C. Wang, J. M. Deng, G. A. Ateshian, and T. H. Clark. An automated approach for direct measurement for two-dimensional strain distributions within articular cartilage. *J Biomech Eng*, 124:557–567, 2002.

[187] A. Watanabe, C. Boesch, K. Siebenrock, T. Obata, and S. E. Anderson. T_2 mapping of hip articular cartilage in healthy volunteers at 3T: a study of topographic variation. *J Magn Reson Imaging*, 26(1):165–171, 2007.

[188] A. Watanabe, Y. Wada, T. Obata, T. Ueda, M. Tamura, H. Ikehira, and H. Moriya. Delayed gadolinium-enhanced MR to determine glycosaminoglycan concentration in reparative cartilage after autologous chondrocyte implantation: preliminary results. *Radiology*, 239(1):201–208, 2006.

[189] J. S. Wayne, K. A. Kraft, K. J. Shields, C. Yin, J. R. Owen, and D. G. Disler. MR imaging of normal and matrix-depleted cartilage: Correlation with biomechanical function and biochemical composition. *Radiology*, 228:493–499, 2003.

[190] F. W. Wehrli, H. K. Song, P. K. Saha, and A. C. Wright. Quantitative MRI for the assessment of bone structure and function. *NMR Biomed*, 19(7):731–764, 2006.

[191] G. H. Welsch, T. C. Mamisch, S. E. Domayer, R. Dorotka, F. Kutscha-Lissberg, S. Marlovits, L. M. White, and S. Trattnig. Cartilage T_2 assessment at 3-T MR imaging: *in vivo* differentiation of normal hyaline cartilage from reparative tissue after two cartilage repair procedures–initial experience. *Radiology*, 247(1):154–161, 2008.

[192] A. J. Wheaton, A. Borthakur, E. Shapiro, R. Regatte, J. Akella, J. Kneeland, and R. Reddy. Proteoglycan loss in human knee cartilage: quantitation with sodium MR imaging- feasibility study. *Radiology*, 231:900–905, 2004.

[193] L. M. White, M. S. Sussman, M. Hurtig, L. Probyn, G. Tomlinson, and R. Kandel. Cartilage T_2 assessment: differentiation of normal hyaline cartilage and reparative tissue after arthroscopic cartilage repair in equine subjects. *Radiology*, 241:407–414, 2006.

[194] W. Wilson, C. C. van Donkelaar, R. van Rietbergen, and R. Huiskes. The role of computational models in the search for the mechanical behavior and damage mechanisms of articular cartilage. *Med Eng Phys*, 27(10):810–826, 2005.

[195] W. Wilson, B. van Rietbergen, C. C. van Donkelaar, and R. Huiskes. Pathways of load-induced cartilage damage causing cartilage degradation in the knee after meniscectomy. *J Biomech*, 36:845–851, 2003.

[196] M. Wong, M. Ponticiello, V. Kovanen, and J. S. Jurvelin. Volumetric changes of articular cartilage during stress relaxation in unconfined compression. *J Biomech*, 33(9):1049–1054, 2000.

[197] Y. Xia. Relaxation anisotropy in cartilage by NMR microscopy (uMRI) at 14- microm resolution. *Magn Reson Med*, 39(6):941–949, 1998.

[198] Y. Xia, J. B. Moody, N. Burton-Wurster, and G. Lust. Quantitative *in situ* correlation between microscopic MRI and polarized light microscopy studies of articular cartilage. *Osteoarthritis Cartilage*, 9(5):393–406., 2001.

[199] E. Yelin and L. F. Callahan. The economic cost and social and psychological impact of musculoskeletal conditions. National Arthritis Data Work Groups. *Arthritis Rheum*, 38(10):1351–1362., 1995.

[200] J. Zuo, X. Li, S. Banerjee, E. Han, and S. Majumdar. Parallel imaging of knee cartilage at 3 Tesla. *J Magn Reson Imaging*, 26(4):1001–1009, 2007.

Kuopio University Publications C. Natural and Environmental Sciences

C 218. Madetoja, Elina. Novel process line approach for model-based optimization in papermaking.
2007. 125 p. Acad. Diss.

C 219. Hyttinen, Marko. Formation of organic compounds and subsequent emissions from ventilation filters.
2007. 80 p. Acad. Diss.

C 220. Plumed-Ferrer, Carmen. Lactobacillus plantarum: from application to protein expression.
2007. 60 p. Acad. Diss.

C 221. Saavalainen, Katri. Evaluation of the mechanisms of gene regulation on the chromatin level at the example of human hyaluronan synthase 2 and cyclin C genes.
2007. 102 p. Acad. Diss.

C 222. Koponen, Hannu T. Production of nitrous oxide (N_2O) and nitric oxide (NO) in boreal agricultural soils at low temperature.
2007. 102 p. Acad. Diss.

C 223. Korkea-aho, Tiina. Epidermal papillomatosis in roach (Rutilus rutilus) as an indicator of environmental stressors.
2007. 53 p. Acad. Diss.

C 224. Räisänen, Jouni. Fourier transform infrared (FTIR) spectroscopy for monitoring of solvent emission rates from industrial processes.
2007. 75 p. Acad. Diss.

C 225. Nissinen, Anne. Towards ecological control of carrot psyllid (Trioza apicalis).
2008. 128 p. Acad. Diss.

C 226. Huttunen, Janne. Approximation and modellingerrors in nonstationary inverse problems.
2008. 56 p. Acad. Diss.

C 227. Freiwald, Vera. Does elevated ozone predispose northern deciduous tree species to abiotic and biotic stresses?
2008. 109 p. Acad. Diss.

C 228. Semenov, Dmitry. Distance sensing with dynamic speckles.
2008. 63 p. Acad. Diss.

C 229. Höytö, Anne. Cellular responses to mobile phone radiation: proliferation, cell death and related effects.
2008. 102 p. Acad. Diss.

C 230. Hukkanen, Anne. Chemically induced resistance in strawberry (Fragaria × ananassa) and arctic bramble (Rubus arcticus): biochemical responses and efficacy against powdery mildew and downy mildew diseases.
2008. 98 p. Acad. Diss.

C 231. Hanhineva, Kati. Metabolic engineering of phenolic biosynthesis pathway and metabolite profiling of strawberry (Fragaria × ananassa).
2008. 80 p. Acad. Diss.

C 232. Nissi, Mikko. Magnetic resonance parameters in quantitative evaluation of articular cartilage: studies on T_1 and T_2 relaxation time.
2008. 83 p. Acad. Diss.